Spring 2024

Monitoring Aerosols With Time Resolution With a Rotating Drum Sampler Using LA-ICPMS for Elemental Analysis

John V. Piorkowski
Bucknell University, jvp007@bucknell.edu

Monitoring aerosols with time resolution with a drum sampler using LA-ICPMS for elemental analysis

by

John V. Piorkowski

A Proposal Submitted to the Honors Council

For Honors in Chemical Engineering

4/30/2024

Approved by:

Adviser: _____

Tim Raymond

Second Evaluator in **major**

_____

Dabrina Dutcher

Acknowledgements

I would like to express my gratitude to my advisors, Professors Dabrina Dutcher and Timothy Raymond, for their years of guidance and support during this research. I would also like to thank another lab member, Laura Sakol for her contribution to this work with LA-ICPMS operations.

Table of Contents

Lists of Figures

List of Tables

Abstract

This thesis presents a comprehensive study on the characterization and application of a rotating drum sampler for air quality monitoring, with a focus on aerosol composition analysis using Laser Ablation Inductively Coupled Plasma Mass Spectrometry (LA-ICPMS). The study aimed to determine (1) the cut-off points of the drum sampler to better understand its performance characteristics and (2) to investigate indoor air quality, specifically within makerspaces on Bucknell University's campus. The research highlighted the novelty of applying LA-ICPMS for time-resolved aerosol composition analysis, demonstrating the potential for low-cost pollution concentration studies. The characterization experiments did not yield expected results, but the results provided valuable insights into the sampler's operation and suggested improvements for future research. The indoor air quality monitoring did not reveal significant diurnal variations in metal aerosol concentrations, suggesting effective ventilation in the studied locations. This work lays the groundwork for future studies on aerosol sampling and analysis, emphasizing the need for further methodological development in LA-ICPMS standards and data processing techniques.

Introduction

The Aerosol Lab in the Chemical Engineering Department at Bucknell University purchased the DRUMAir sampler in 2019 from DRUMAir LLC. The 4 drum sampler used in these studies is nominally based on the Davis Rotating Unit for Monitoring (DRUM), developed by researchers at UC Davis. While the DRUM unit had better characterization regarding its performance of monitoring, the 4 drum sampler did not have robust documentation regarding the expected performance and characterization of the instrument. The research conducted in this thesis is one of the first attempts made at using LA-ICPMS to investigate the composition of collected aerosols with time resolution. This novel application had the potential of being a relatively low cost analysis of pollution concentration.

The contents of this thesis involve two main objectives: (1) experimentally determine the cut-off points of the drums to characterize the instrument for future use, and (2) investigate the indoor air quality of the on campus makerspaces on Bucknell's campus with elemental and time resolution, one of the first of its kind.

The beginning of this thesis' work involved an investigation of instrument operation. A year (Fall '21 and Spring '22) was spent trying to troubleshoot the normal operation of the instrument, both the controlling software and physical hardware of the system. After thorough testing of the mechanical workings of the instrument, it was determined that there was a critical error with the electrical and code that ran the instrument. From here, it was shipped back to the manufacturer, who was able to repair it.

The next year (Fall '22 and Spring '23) was spent in collecting and analyzing data collected by the instrument when deployed in on campus makerspaces. Through coordination with the makerspaces, the instrument was run and the collected strips went for ICP-MS analysis. Laura Sakol was a lab member who was trained on the ICP-MS, and ran samples on the instrument and also was involved in the data collection in the makerspaces. Fall '23 was spent developing methods to experimentally determine the cutoff points of the instrument. Spring '24 was spent running the experiments, data collection by Laura in the ICP-MS, and data analysis.

Background

Despite its importance, air quality is often overlooked. Air pollutants are often invisible and odorless, making them less noticeable compared to other environmental hazards. Also, consequences of poor air quality may not manifest immediately, with health and environmental impacts taking years to show. The long time scale makes the effects of particulate matter often blamed on other factors, such as heart attacks and asthma. Due to the complexity of competing interests of involved parties, economic interests, and political considerations may divert attention away from air quality concerns.

Poor indoor and outdoor air quality exposure can cause various health effects. Dockery (1993) investigated the mortality rates of exposure to poor air quality, linking particulate matter and sulfates as the most harmful. Pope (2000) probed the corresponding biological pathways, chronic exposure, and specific health effects of particulate matter exposure. Throughout the years, ongoing research has linked many health conditions to exposure to fine particulates in the air such as cancer, respiratory diseases, dementia, and heart disease (NIH, 2023 and Zhang et al., 2023). Different kinds of aerosols are found in a range of different sizes. An overview of these sizes can be found in **Figure 1.**

Particle Diameter, μm

	0.001	0.01	0.1	1	10	100	1000

Measurement Scale	Angstrom	1nm 10⁻⁹m	10nm 10⁻⁸m	100nm 10⁻⁷m	10⁻⁴cm 10⁻⁶m	10⁻³cm 10⁻⁵m	10⁻²cm 10⁻⁴m	0.1cm 10⁻³m
Designated Size Ranges		← Nanometer →	← Submicrometer →		← Micrometer →			
				Fine		← Coarse →		
			Ultrafine					
		← Free Molecule →		Transition		Continuum Region		
Aerosol Definitions			Fume			Dust		
						Fog, Mist		
		Smog				Spray		
		Smoke			Cloud Droplets			
Typical Aerosol Size Ranges		Metal Fumes			Cement Dust			
		Sea Salt Nuclei			Coal Dust			
					Flour			
		Oil Smoke			Coal Fly Ash			
				Machining Fluids				
		Tobacco Smoke						
		Diesel Smoke			Paint Spray			
	Atmospheric Aerosol	Nuclei → Accumulation Mode → Coarse Particle Mode						
Typical Bioaerosol Size Ranges		Viruses		Bacteria	Pollen			
				Fungal Spores				
Sampling Definitions			PM-10					
			PM-2.5					
			Thoracic Particles					
			Respirable Particles					
Wavelength of Electromagnetic Radiation		X-Rays	Ultraviolet	Visible	Infrared			
				Solar				
Other	Gas Molecules		Mean Free Path (STP)		Red Blood Cell	Human Hair		
						Visible to Eye		
			Proteins		Std. Sieve Opening	400 200 100 60 40 20		

Figure 1. Particle size ranges and general definitions of aerosols. Adapted from Aerosol Technology (pg. 9), by W. Hinds, 1999, John Wiley & Sons.

Heavy metal particles in the air are particularly harmful to human health. Studies have shown that welders have an increased risk of loss of smell due to the aerosolized heavy metals in the air (Antunes et al., 2007). Welding fumes contain aerosolized heavy metals, including manganese and zinc, both of which are found to damage olfactory nerves and cause loss of smell (Iannili et al., 2016 and Jafek et al., 2004). These aerosolized metals vary in size, but the smaller the particle, the more likely it is to penetrate the myelin sheath. The myelin sheath is a protective layer around a nerve, and

select molecules or particles can transport through it, causing damage to the olfactory nerve, and thus causing a loss of smell. Therefore, it is crucial to be able to monitor air quality and identify both the elements present and their size in air samples over time.

During the 2020 COVID-19 pandemic, there was a large focus on improving indoor air quality. Virus particles vary in size, but are highest in concentration at roughly 100 nm, or 0.1 μm. Efforts were made to buy air purifiers that utilize HEPA filters, which can filter 99.97% of all particles that are 0.3 μm. This size is the hardest to filter because 300 nm particles are just large enough that Brownian motion is becoming less of a diffusive effect, but just small enough that direct impaction and settling is worse at removing them, creating a minimum of particle filtration at 300 nm. While these filters are great at removing most contaminants, some smaller nanoparticle sized aerosols are only partially removed using these techniques. The smaller that particles are, the deeper they can penetrate into the lungs or nasal cavities of humans, and from there, they are more likely to enter the bloodstream (Saleh et al., 2019) (**Figure 2**).
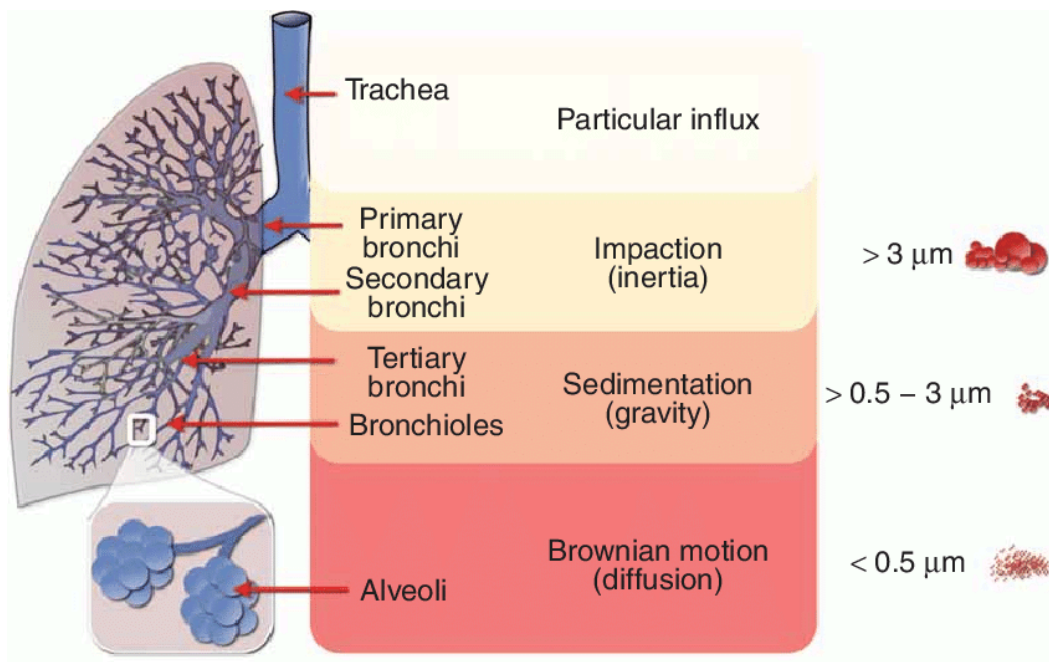
Figure 2. Penetration of different aerosol sizes and their main method of removal in the human respiratory tract. Adapted from Klinger-Strobel M et. al., 2015.

Continuous monitoring of pollution is a challenging task. The monitors cannot detect more than one or two distinct species. When filtration or impaction is used, ex post facto, or retroactively, analysis of collected aerosols requires specialized and expensive equipment. A solution to some of these shortcomings of continuous monitoring systems is solved by passive rotating drum samplers. Rotating drum samplers use a cascade of drums that collect aerosols of different sizes using particle impaction. A pump pulls air through the inlet and around the drums. These drums rotate at a fixed rate so that the size separated aerosols can be tracked to a specific time that it was collected at. These drum samplers have a much lower cost than continuous monitoring systems and can be

deployed in remote locations due to their low power consumption. The rotation rates of the drums can be set such that a sampler can be deployed for up to two months. Additionally, if implemented, LA-ICP-MS offers a much cheaper method of analysis of collected particles, when compared to other methods of elemental speciation.

Rotating drum samplers work on the theory of particle impaction. Particle impaction leverages the inertia to separate aerosols of different mass. A 90° bend is put into the aerosol steam before each drum stage. Aerosols with more mass have more inertia, which is resistance to changing the direction of motion. Larger and more massive particles have greater inertia and are less influenced by changes in gas flow, making them more likely to impact onto collection surfaces. This is the same concept that makes smaller, lighter vehicles easier to accelerate, decelerate and maneuver when compared to large, heavy trucks. Analogously, larger aerosol particles are less likely to follow the change in gas flow around the 90° bend, and impact the side of the drum. A cross-sectional view of an impactor is shown below in **Figure 3.**
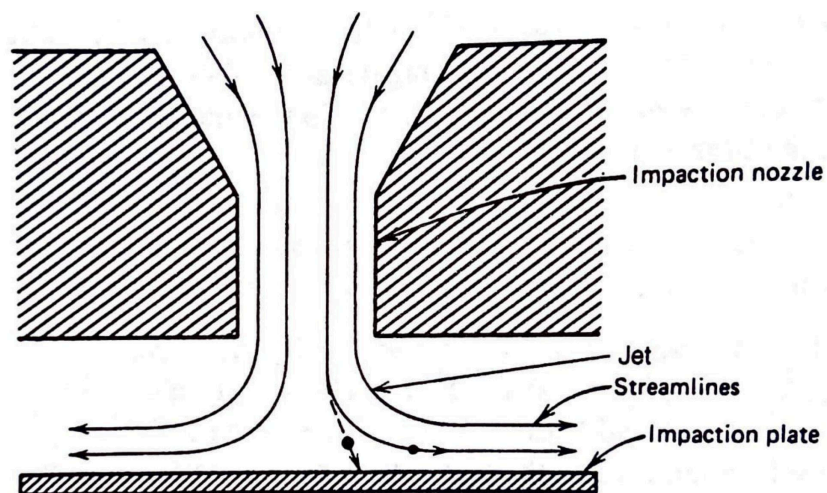
Figure 3. Cross-sectional view of an impactor. Adapted from Aerosol Technology (pg. 122), by W. Hinds, 1999, John Wiley & Sons.

Particles are separated by size as they travel through the impactors. An experimental investigation is what will be outlined in the characterization portion of this thesis. There are theoretical and empirical mathematical relationships between the parameters of the impactor and the cutoff point of collection. The cutoff point is defined as the size where at least 50% of the particles at that size are collected on the impaction plate. A comparison of the theoretical and actual collection cut-off curves is displayed below in **Figure 4.**
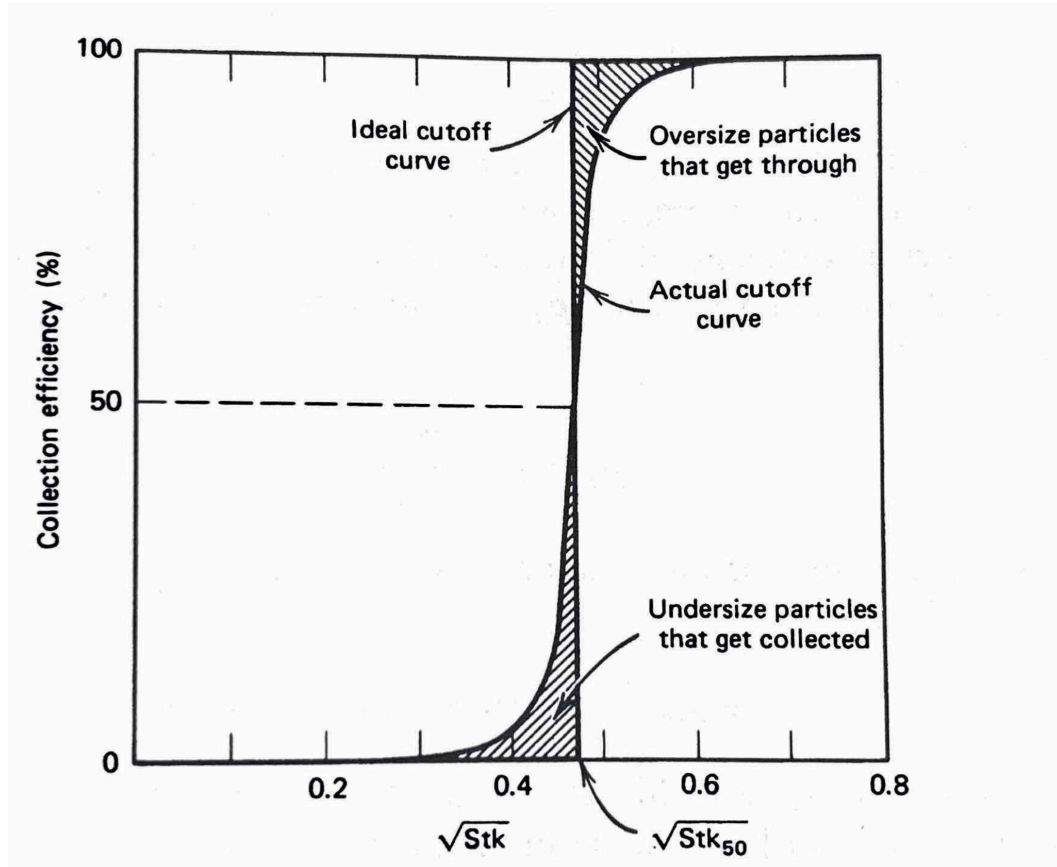
Figure 4. Comparison of theoretical and actual cutoff points, as a function of the root of Stokes number. Adapted from Aerosol Technology (pg. 125), by W. Hinds, 1999, John Wiley & Sons.

To find the theoretical cutoff point of a rectangular impactor, the following equation, **Equation 1**, is used.

$$d_{50}\sqrt{C_c} = \left[\frac{9\eta W^2 L (Stk_{50})}{\rho_p Q} \right]^{0.5} \qquad \textbf{Eq. 1}$$

Where:

d_{50} = the cut-off point, where 50% of particles that size are impacted

C_c = Cunningham correction factor

η = dynamic viscosity

W = width of the rectangular cut

L = length of the rectangular cut

Stk_{50} = Stokes number for 50% collection efficiency. For impactors that are

      meeting recommended design criteria, this is 0.59

ρ_p = density of the particles. For aerodynamic diameters, this is 1 g/mL

Q = flow rate through the nozzle

An empirical correlation between $d_{50}\sqrt{C_c}$ and d_{50} is given in **Equation 2.**

$$d_{50} = d_{50}\sqrt{C_C} - 0.078 \qquad\qquad \textbf{Eq. 2}$$

      In a cascade impactor, there are sequential impaction plates that have decreasing orifices to collect smaller particles as the aerosol stream progresses, shown below in **Figure 5**. Marple (1970) thoroughly investigated the ideality of impactors, providing design criteria that are used in the construction of aerosol impactors and investigating the theoretical cutoff points of collection nozzles. Raabe (1975) investigated the deposition

locations of varying sizes of aerosol particles. Particles that are larger (0.52 - 1.04 μm)

deposit in the upper respiratory tract and smaller particles (<0.01 μm) deposit further

into the pulmonary regions. Utilizing an impactor, Cahill (1977) was able to separate a

generated aerosol stream by size to make a representative mixture of sizes that would be

harmful to human health. Extending this work, this thesis aims to see if the rotating drum

instrument can capture the small particles that could damage the olfactory nerve.
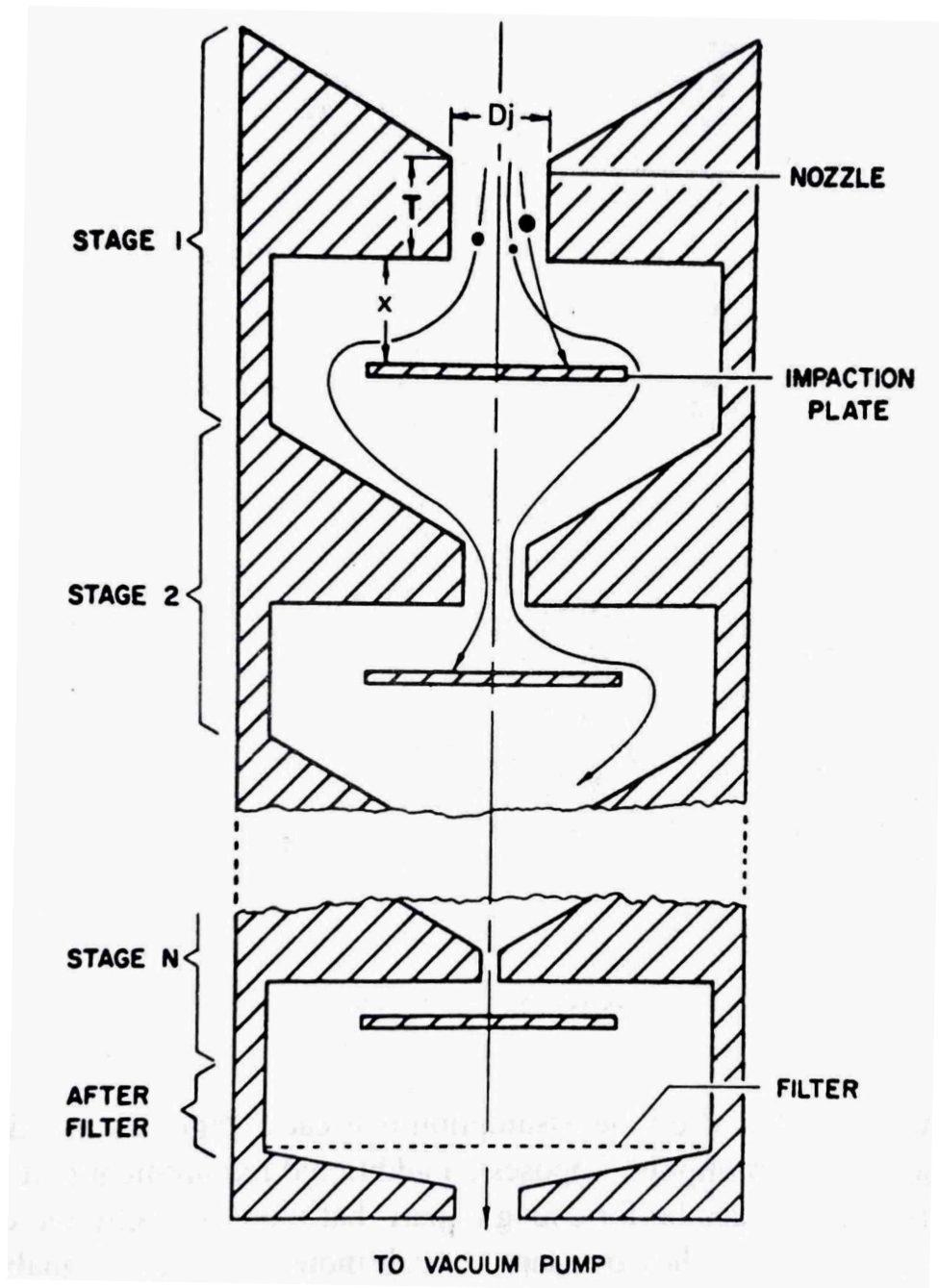
Figure 5. Schematic of a cascade impactor. Adapted from Aerosol Technology (pg. 129), by W. Hinds, 1999, John Wiley & Sons. Copyright 1979 by the Board of Regents of the State of Florida.

Generated aerosol particles using a constant output atomizer generally follow a log-normal size distribution, which means that a range of particle sizes will be generated. There are two main types of aerosol size classifications, aerodynamic size and mobility size. Aerodynamic size is defined as the diameter of a sphere with density 1 g/cm³ which will settle in still air at the same velocity of the particle. This measure is useful to find a spherical equivalent diameter of irregularly shaped particles. An illustration of how the true diameter of an irregular particle is related to aerodynamic size is shown below in **Figure 6.**
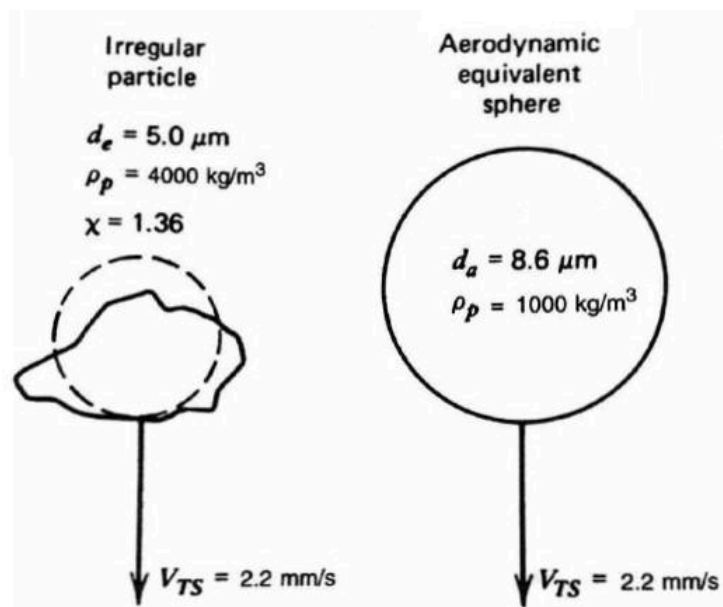

Figure 6. Comparison of an irregular particle to an aerodynamic size with the same settling velocity. Adapted from Aerosol Technology (pg. 54), by W. Hinds, 1999, John Wiley & Sons.

Mobility size is the equivalent diameter of a spherical particle that has the same electrical mobility, or ability to move in response to an electric field, of an irregularly shaped particle. Because of these different classifications, it is possible for a particle to have more than one size. There are several other kinds of size that the same particle can have, some of which are highlighted in **Figure 7.**
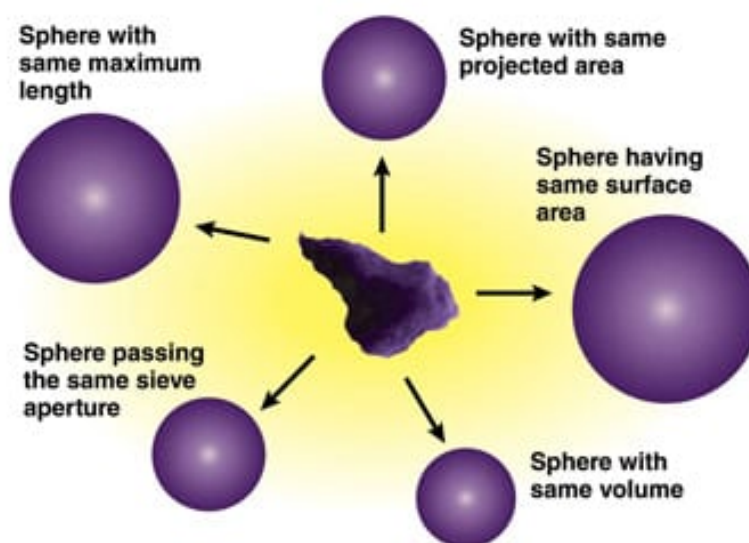

Figure 7. Explanation of the different kinds of equivalent diameters that an irregular particle can have.

If we assume that the generated particles are spherical and have uniform density, the aerodynamic and mobility sizes will be very close. This is a common assumption made in aerosol science, and it is reasonable, as the generated aerosols in this experiment have consistent composition (and densities). Additionally, the aerosols generated in this

experiment are fairly spherical, especially compared to other types of particulate matter, such as soot, which commonly has a fractal shape.

The DMA operates on the principle of electrical mobility. All aerosol particles have an ability to mobilize, or change their direction, in the presence of an electric field. The aerosols are charged with a krypton source, and flow is passed along an electric plate, as seen in **Figure 8.** The electrical mobility of a particle depends on its size and charge. Larger particles have lower electrical mobility compared to smaller particles, given the same charge. Therefore, as particles move through the DMA, smaller particles with higher electrical mobility are able to traverse the varying electric field and reach the detector or collector more easily than larger particles with lower mobility. Using a DMA, the voltage can be selected such that a narrow selection of particle sizes pass through the instrument.
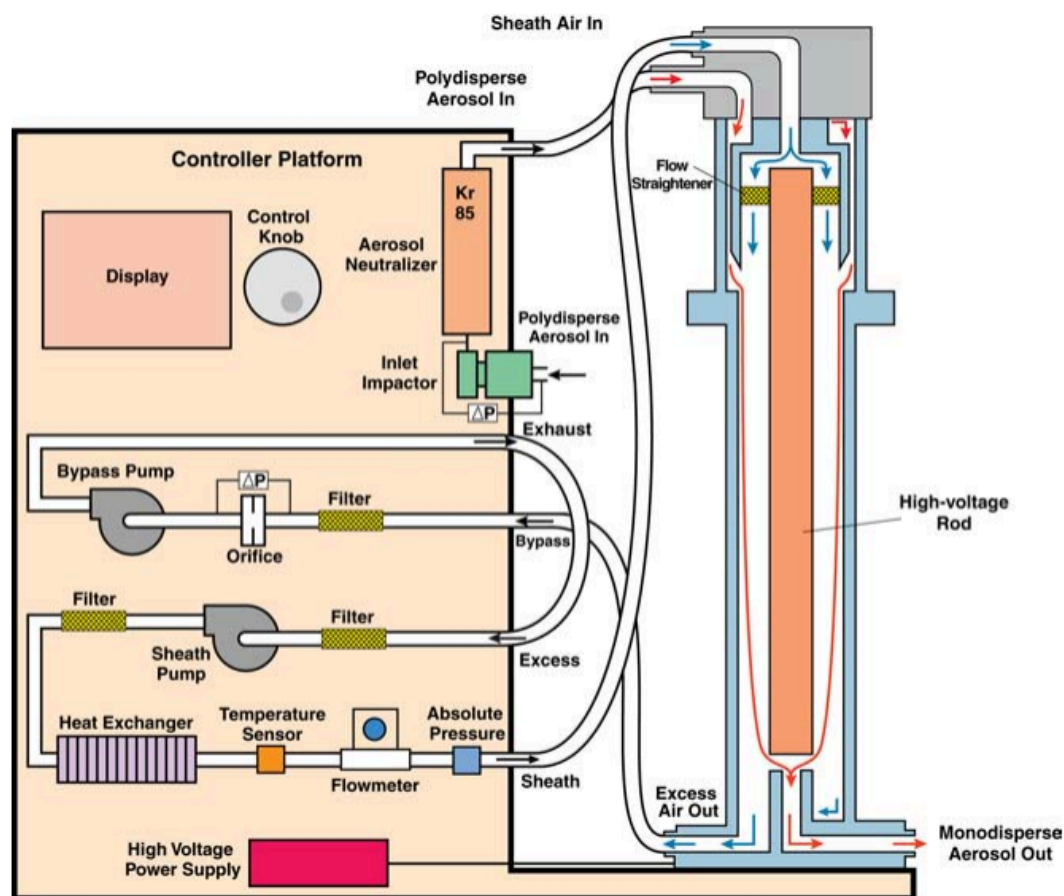
Figure 8. Schematic of a differential mobility analyzer (DMA). Adapted from Series 3080 Electrostatic Classifiers Operation and Service Manual by TSI, 2006

When a DMA is used in tandem with a condensation particle counter, or CPC, a distribution of sizes can be found in a generated aerosol stream. This configuration is called scanning mobility particle sizer, or SMPS. CPCs operate by enlarging them through condensation of a vapor and then counting them optically, as seen in **Figure 9.** When operated in SMPS mode, the CPC counts the particles exiting the DMA, as the DMA's voltage is digitally controlled, thereby counting particles of a certain size. As the

whole range of particles is scanned, the Aerosol Instrument Manager (A.I.M.)

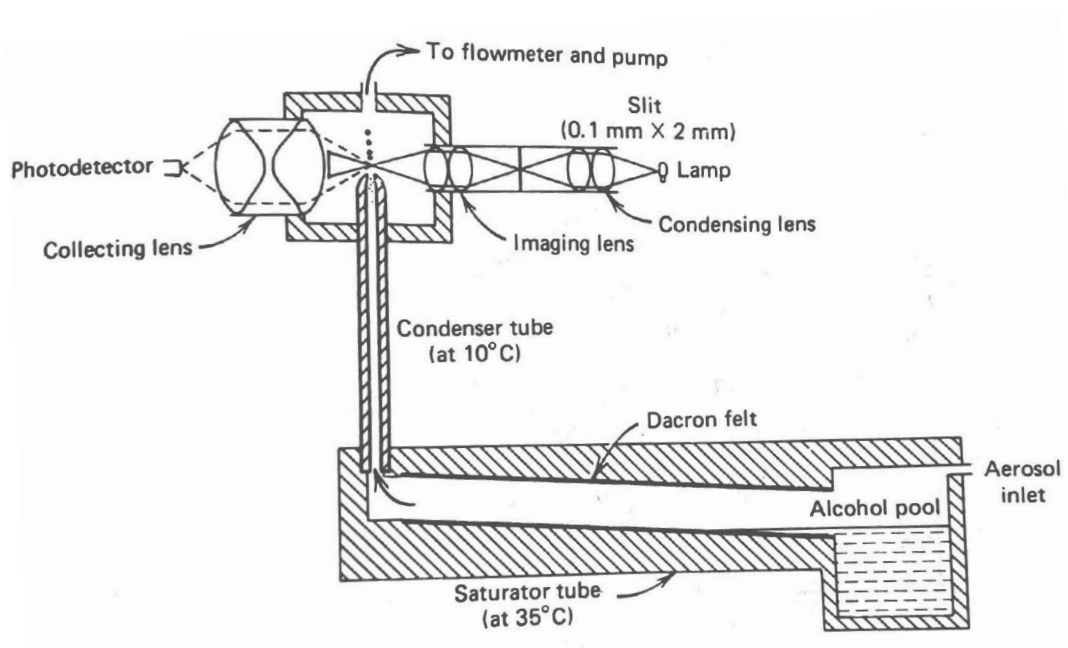coordinates the data collection from both instruments.

Figure 9. Schematic of a condensation particle counter (CPC). Adapted from Aerosol

Technology (pg. 297), by W. Hinds, 1999, John Wiley & Sons. Originally from Agarwal,

J. K., and Sem, G. J. (1980).

The method of analysis used on collected strips of data is a laser ablation

inductively coupled mass spectrometer (LA-ICPMS). In this method of analysis, a laser

instrument and ICPMS instrument work in sync to provide an analysis of elemental

concentration over time. Fabretti (2007) used ICPMS to analyze elemental composition

of particulate matter collected near roadways. A laser is programmed to move in a

straight line along the strip of collected aerosols. As the laser moves along the strip, it ablates material in discrete spots from the medium to form a collection of vapor and particles. The spots that are formed on the mylar medium from the laser are shown in **Figure 10,** and have a diameter of 0.2 mm. This collection is then ionized in an inductively coupled plasma torch, which generates a high temperature plasma full of distinct charged atoms. The ions are separated based on their mass to charge ratio, and the ion signals are detected, generating a mass spectrum of an individual element.

Figure 10. Shows a laser ablated mylar strip. The dots down the center are where the laser spot hit. The spots are around 0.2 mm in diameter.

Instrumentation

The drum sampler is manufactured by DRUMAir LLC and is the 4 drum model, shown in **Figure 11.** As described in the Introduction section, there is little information regarding the characterization of the instrument. A general schematic of the instrument can be seen below in **Figure 12**. During the characterization experiments, a vacuum was pulled behind the fourth drum to achieve the critical flow. During the normal use operation, a 0.5 hp vacuum pump, manufactured by GAST, was used to achieve critical flow. The aerosols are collected on a mylar strip, which is a polyethylene terephthalate film that is used as the aerosol medium.
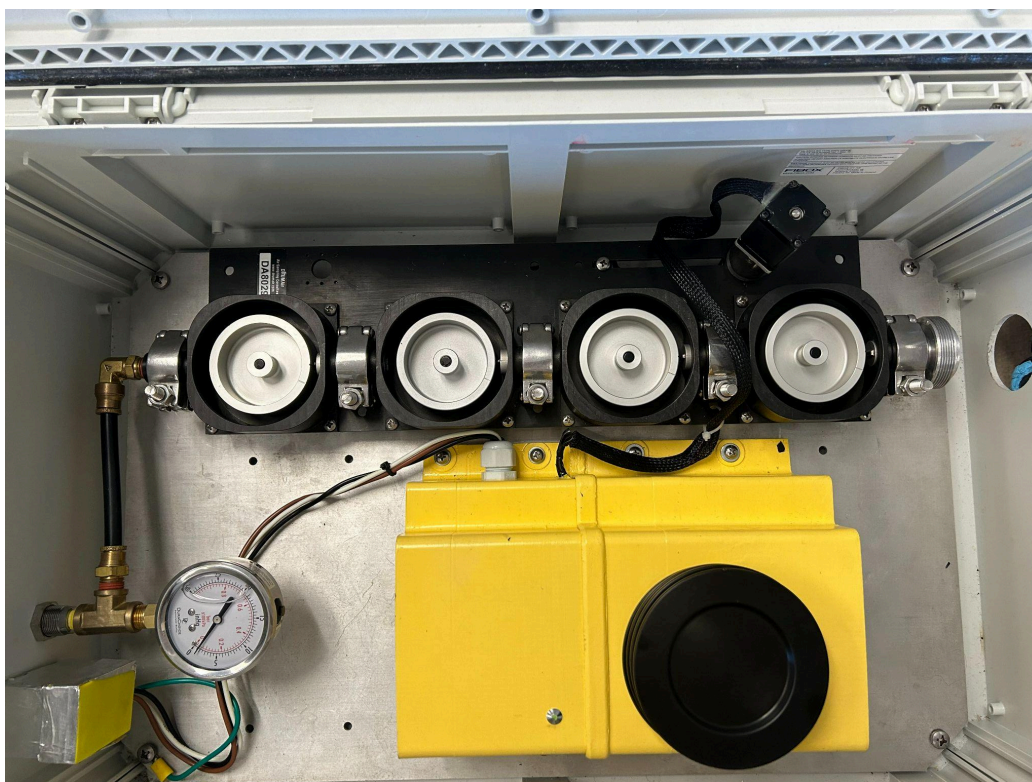
Figure 11. Photo of the 4 drum rotating drum sampler purchased from DRUMAir LLC.
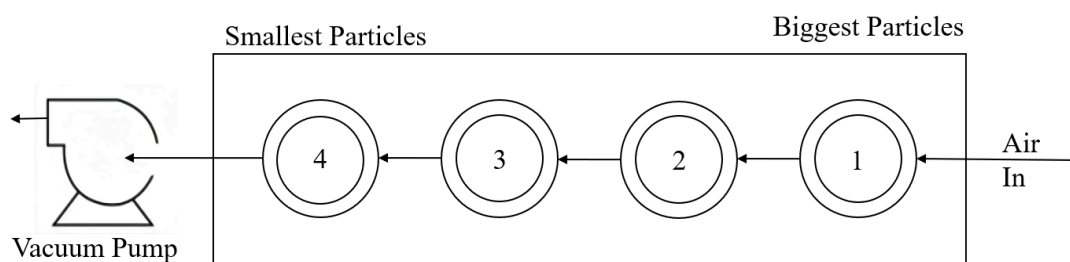

Figure 12. Simplified schematic of the 4 drum rotating drum sampler purchased from DRUMAir LLC.

The 4 drum rotating sampler used in this experiment has specific orifice and operating sizes listed below in **Table 1.** In addition to these design specifications, the drum operated with a critical flow of 23 L/min and all cut lengths are 9.5 mm.

Table 1. Design specification of the 4 drum sampler: collected particle sizes and orifice width for the different drum stages.

Drum #	Collected Particle Sizes (µm)	Orifice Width (cm)
1	> 3	0.193
2	3.0 - 1.2	0.082
3	1.2 - 0.34	0.030
4	0.34 - 0.15	0.028

The strip is expected to look like the strips shown below in **Figure 13.** The particular data shown on strips is particulate matter from near a California railyard. Dirty air should appear as a solid line across the length of the strip. Although this is not what our strips appear to look like, the dark lines can be imagined as our collected aerosols that are being scanned for in LA-ICPMS.

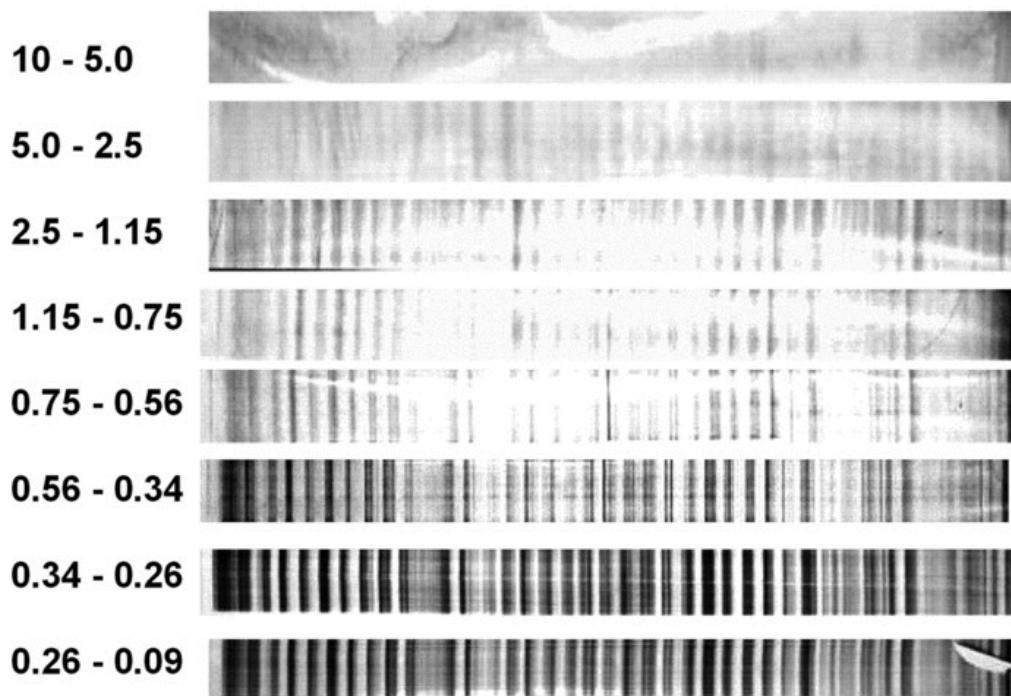## DELTA Group 8 DRUM, Denio site

Figure 13. Collected particulate matter on a rotating drum sampler. Adapted from T. A. Cahill et al., 2010.

The syringe pump used to feed the solution was an inovenso (Model: IPS-14RS). To aerosolize the salt solutions, the solution was fed to a TSI Constant Output Atomizer (Model: 3076) was supplied with air by a TSI Filtered Air Supply (Model: 3074B). Generated aerosol particles were dried by a silica gel and zeolite diffusion driers in series.

To verify the aerosol size distribution in the characterization experiments, a TSI differential mobility analyzer (DMA) (Model: 3080) was used in scanning analog control mode in series with a TSI Condensation Particle Counter (CPC) (Model: 3775).

To select the desired particle size in the generated aerosol stream, the TSI DMA (Model: 3080) was operated with a sheath flow rate of 5 lpm. Using panel control, a specific voltage was applied to control the size of the aerosols entering the drums.

The laser ablation unit is a NWR 193 LA manufactured by Elemental Scientific and is controlled by the ActiveView 2 software. The laser fire was set to burst mode and was at 50% fluency, and spot size was set to "large" (~0.2 mm). The ICP-MS unit is a iCAP-RQ ICP-MS manufactured by ThermoScientific and is controlled by Qtrega software. The software was used to control the path of a laser down the length of the mylar strip The software was used to match the experiment duration from the path of the laser.

Methods

Characterization

A sample aerosol stream of a distinct metal was generated at the TSI constant output atomizer using a pressurized air stream and a solution of a metal salt in aqueous solution. A distinct metal was used for each size, so the signal from the ICP-MS matches to a specific size. The aerosol was sent through two sequential absorption columns for drying, silica gel and zeolite. Before selecting the size using the DMA, the size distribution of the generated aerosols was checked using the SMPS configuration, as shown in **Figure 14**, to verify that the selected size was in the distribution.
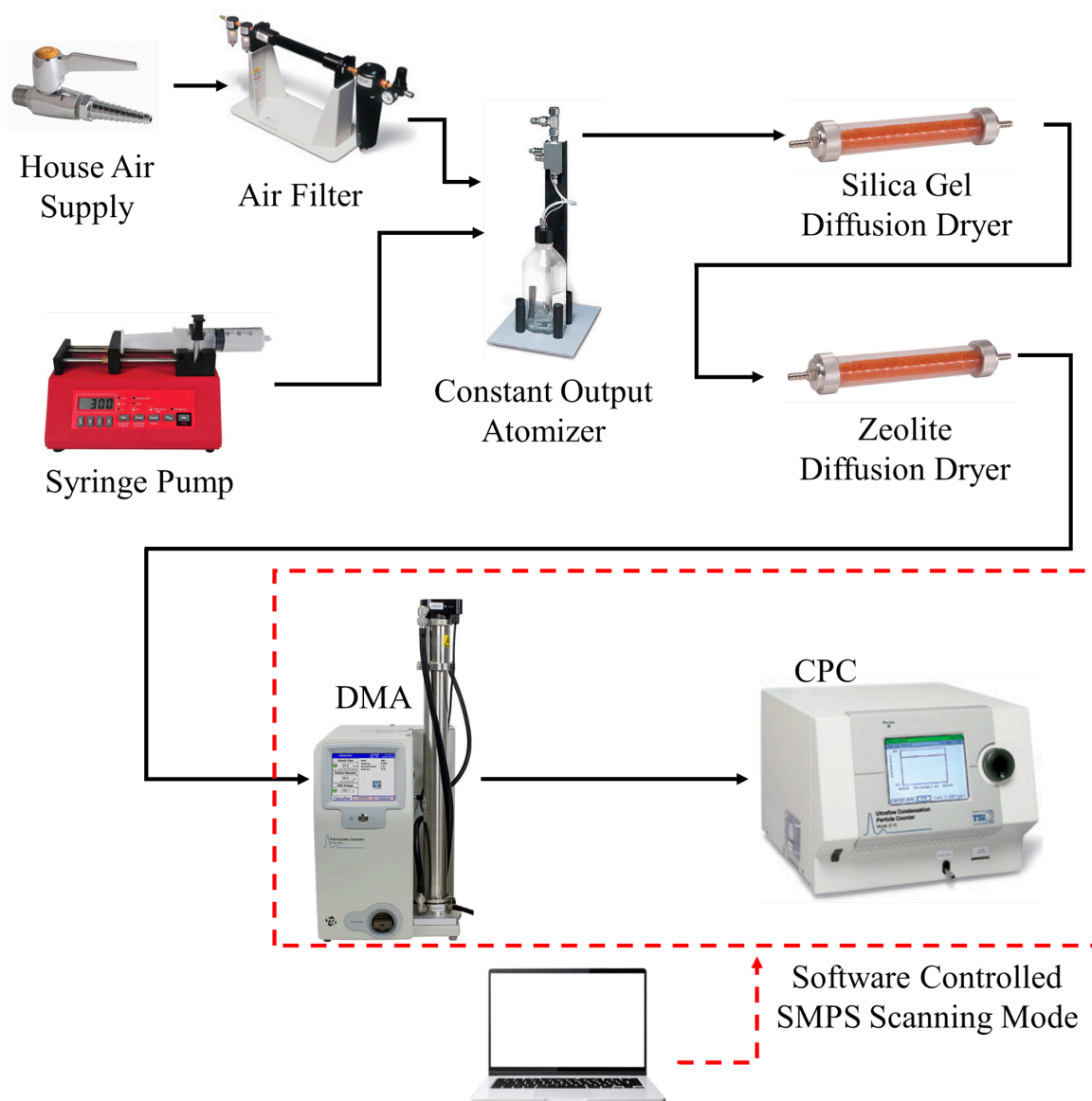
Figure 14. Experimental scheme for verifying the particle size distribution of generated

aerosol before the characterization procedure. The generated aerosol is dried and the

Aerosol Instrument Manager software is used to synchronize the DMA and CPC for

SMPS mode.

After the SMPS configuration was checked, the stream was diverted to the DMA in size selection mode, which allowed certain sized particles to continue the flow through the stream, while all other particles were separated using electrical mobility. The stream was supplied with additional air from a filtered pressure equilibration vent and continued to the rotating drum sampler. Each drum was wrapped in mylar to collect impacted particles (**Figure 15**). The house vacuum line was pulled on the end of the drum sampler to achieve critical flow through the instrument. This setup is outlined below in **Figure 16**.

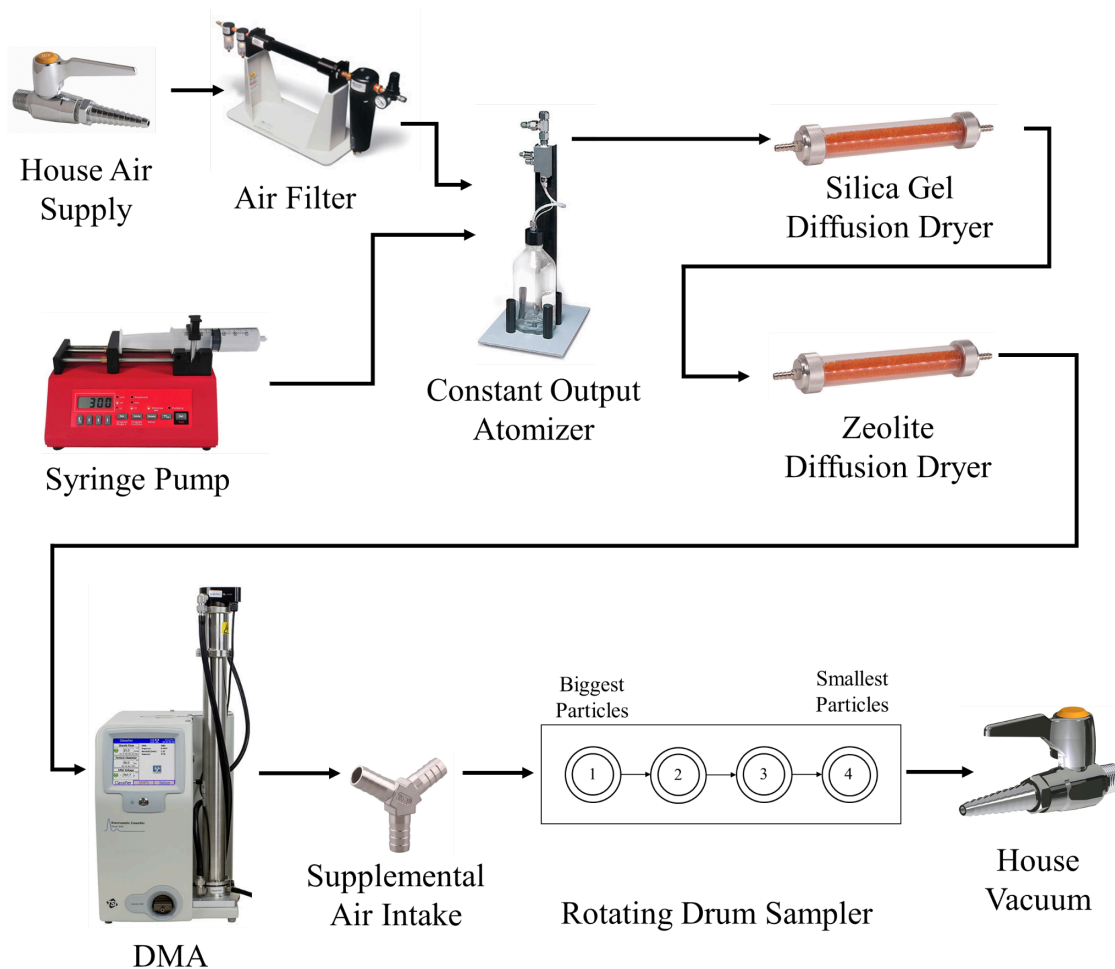**Figure 15.** One of the drums wrapped in the mylar collection medium

Figure 16. Experimental scheme of the characterization procedure. Generated aerosols are dried and size selected before impaction on the sampler.

After collection, the mylar strips were transferred to sample holders for the LA-ICP-MS. The data collected from each strip was stored in a .csv file and were analyzed and plotted in MATLAB.

Using **Equations 1** and **2** and the parameters given by the manufacturer, a
theoretical cut-off point can be calculated and compared to the expected manufacturer
cut-off point. Substituting **Eq. 1** into **Eq. 2** yields the following **Equation 3**:

$$d_{50}(\mu m) = \left[\frac{9\eta W^2 L(Stk_{50})}{\rho_P Q} \right]^{0.5} - 0.078 \ \mu m \qquad \textbf{Eq.3}$$

Solving **Equation 3** with the drum sampler parameters gives theoretical cut-off
points, which are compared to the manufacturer provided cut-off points in **Table 2.**
Sample calculations are provided in **Appendix A**.

Table 2. Comparison of theoretical cut-off points as calculated and manufacturer
information of cut-off points.

Drum #	Manufacturer Cut-off Points (μm)	Calculated Cut-off Points (μm)
1	3	2.91
2	1.2	1.19
3	0.34	0.39
4	0.15	0.20

The calculated values are consistent with the manufacturer's cut-off points, but
begin to vary at lower cut sizes. Therefore, during the characterization experiments,
determining the cut-off point of the drums that collect the smallest particles will be the
main focus.

The distinct metal salts, the size they were selected at, and the position that they were collected on the drum is shown below in **Table 3.** The concentration of the solutions were varied to ensure that the peak of the aerosols in the log normal distribution was near the selected size.

Table 3. Information on the size tracking metal salts used.

Salt	Concentration (g/L)	Size (nm)	Position (mm)
Aluminum Sulfate	2.5	50	0
Iron Chloride	2.7	100	34
Copper Sulfate	3.2	150	68
Nickel Sulfate	4.5	200	102
Lanthanum Nitrate	5.5	250	136

Indoor Air Quality Investigation

The drum sampler was run for around 1 week in three locations on campus: the kiln room at the 7th Street Makerspace, the Project Development Lab (PDL) in Dana Engineering, and outside on the rooftop of Academic East. The aerosols were collected on mylar strips and were run in the ICP-MS. Elemental signals were averaged for a final reporting of average signal of element per week to determine elements whose time resolutions were worth investigating.

Results

Characterization

The following **Figures 17 - 23** show the elemental signal over the length of the strip. The x-axis is normalized by dividing each position by the final position, which was done due to inconsistent laser run times in the ICP-MS. All units presented in the results section are arbitrary units. Most of the spike has been cut out of the plotted data, but artifacts of it still remain. In all of the annotated figures below, the red arrows indicated where the expected signal peak should be and the blue arrows indicate spikes that are artifacts of the ICPMS signal spike at the beginning of the strips. $x = 0$ indicates the beginning of the strip and $x = 1$ indicates the end of the strip.

The time axis could be converted to actual time through mathematical transformation and the signal axis could be converted to concentration using the ICPMS standards. This was not done for any of the datasets due to the lack of structure in the data, as discussed in the **Discussion** section. It is important to note that there are no peaks correlating to impacted metal ions as expected. An in depth analysis of this is presented in the **Discussion** section. Additional plots are presented in **Appendix A** in **Figures A1 - A7.**

Figure 17 shows the smallest particles that were run in the characterization experiments at 50 nm . Artifacts from the LA-ICPMS signal spike are present at the beginning of Drums 1 and 3, as depicted by the blue arrows. The aluminum salt was

impacted on the drum near the beginning of the strip, so any peak should be close to 0 on the normalized x-axis. Based on the calculated and manufacturer cut-off sizes, there should not be many 50 nm particles collected on the drums. If a peak were to appear anywhere, it should be on Drum 4, as indicated by the red arrow. There is no signal present where it is predicted to be, but this is reasonable because the size of the particles are much lower than the cut-off points that are predicted.
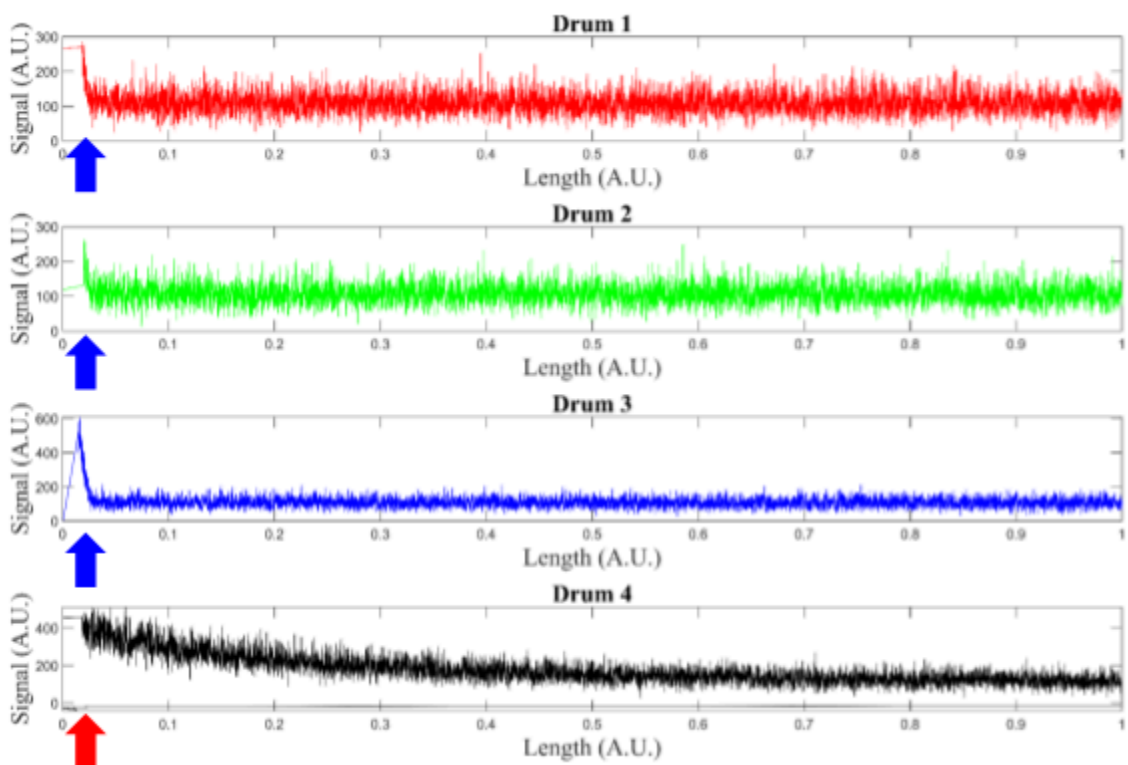

Figure 17. Aluminum signal intensity down the length of the mylar collection strip. Aluminum particles' mobility size was 50 nm. Blue arrows indicate artifacts of the ICPMS signal spike, and red arrows indicate where the expected peak should be.

Figure 18 shows the signal for chlorine. At a size of 100 nm, there should not be much collected material, as it is still below what the cut-off points are expected to be. If anywhere, there should be a signal spike at x = 0.2 on Drum 4, as indicated by the red arrow.
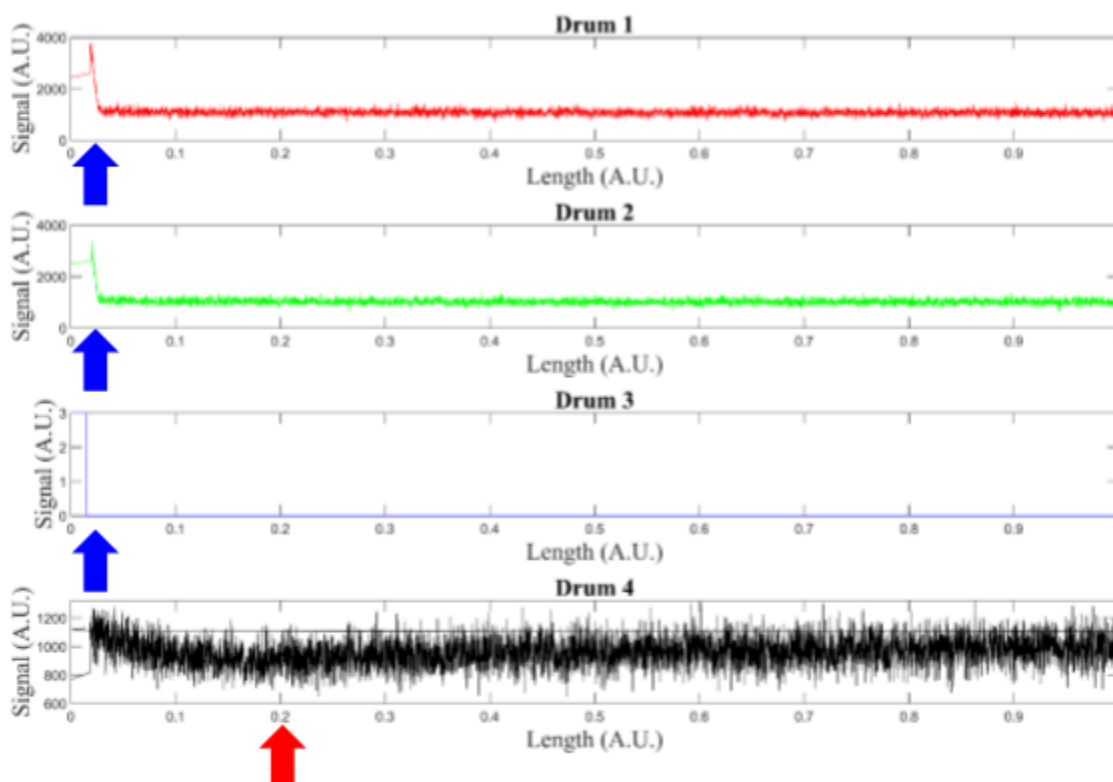

Figure 18. Chlorine signal intensity down the length of the mylar collection strip. Chlorine particles' mobility size was 100 nm. Blue arrows indicate artifacts of the ICPMS signal spike, and red arrows indicate where the expected peak should be.

Similarly to **Figure 18, Figure 19** shows the signal for 100 nm iron particles. The peak should be in the same place because the metal salt that was used was iron chloride. There is still no peak present for the 100 nm particles on Drum 4, which might indicate that they are not impacting on the mylar strip, or that there is not enough impaction happening to generate a signal spike. There is still a signal spike at the beginning of the strips, as shown by the blue arrow.
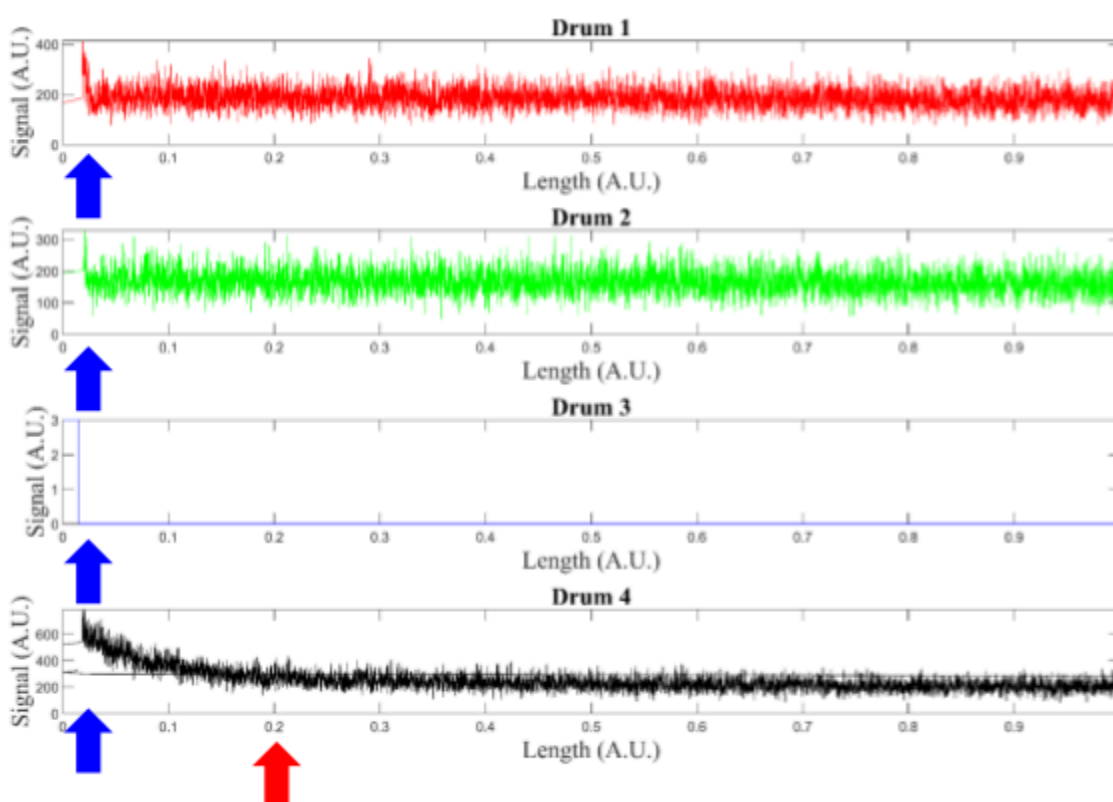

Figure 19. Iron signal intensity down the length of the mylar collection strip. Iron particles' mobility size was 100 nm. Blue arrows indicate artifacts of the ICPMS signal spike, and red arrows indicate where the expected peak should be.

Figure 20 shows the signal observed for copper, which was size selected at 150 nm. By this size, there should be some impaction on Drum 4 around x = 0.4. There is no signal spike present. However, the cut-off point calculated with **Eq. 3** predicted that 200 nm is the largest particle that will be impacted on Drum 4.
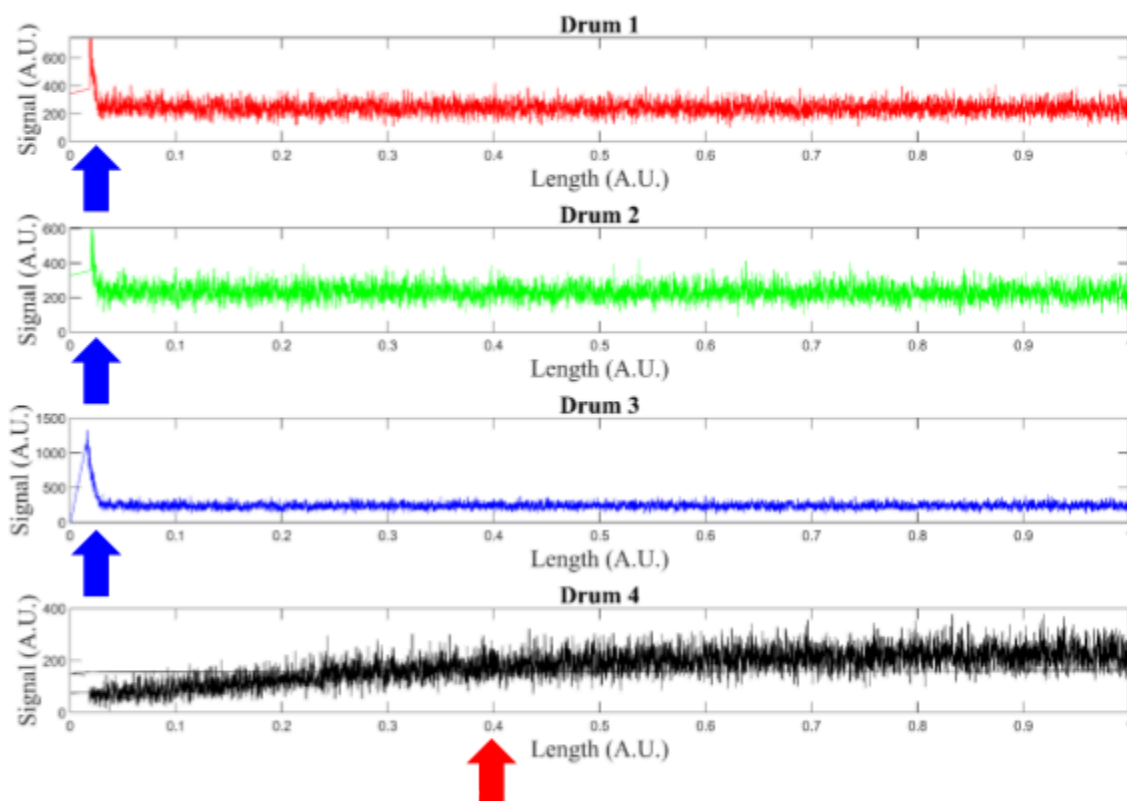

Figure 20. Copper signal intensity down the length of the mylar collection strip. Copper particles' mobility size was 150 nm. Blue arrows indicate artifacts of the ICPMS signal spike, and red arrows indicate where the expected peak should be.

Figure 21 shows the signal for sulfur down the length of the strip. Because sulfate was a common counterion in the metal salt solutions, there are several locations where there can be a sulfur peak, denoted by the red arrow. The most probable peak to be there would be a x = 0.8, because its size was 200 nm, which according to the cut-off points should be impacted on Drum 4. Still, there are no signal peaks present.
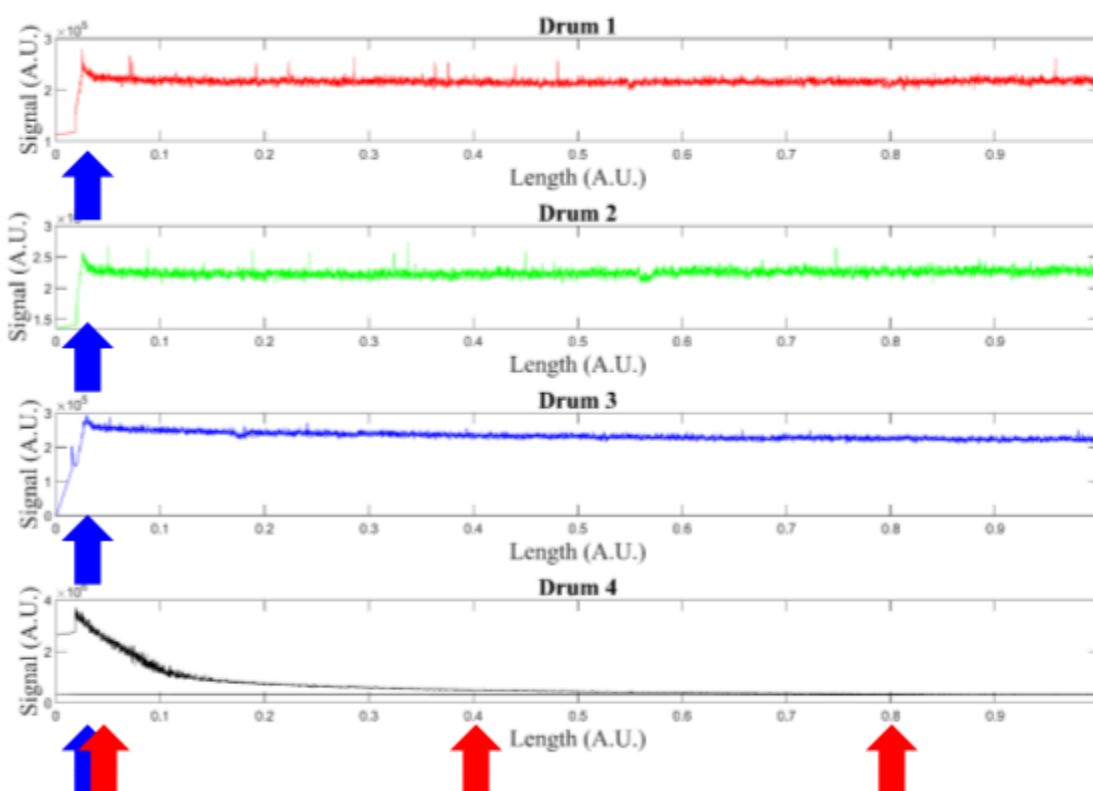

Figure 21. Sulfur signal intensity down the length of the mylar collection strip. Sulfur particles' mobility size was selected at 50 nm, 150 nm, and 200 nm. Blue arrows indicate artifacts of the ICPMS signal spike, and red arrows indicate where the expected peak should be.

Figure 22 shows the nickel signal on the collected drums. At a size of 200 nm, a signal peak should be present on Drum 4 at x = 0.8. There is no peak present, which means that there are very few particles making it through the DMA and to the drum sampler. An explanation of this is presented in the **Discussion** section.
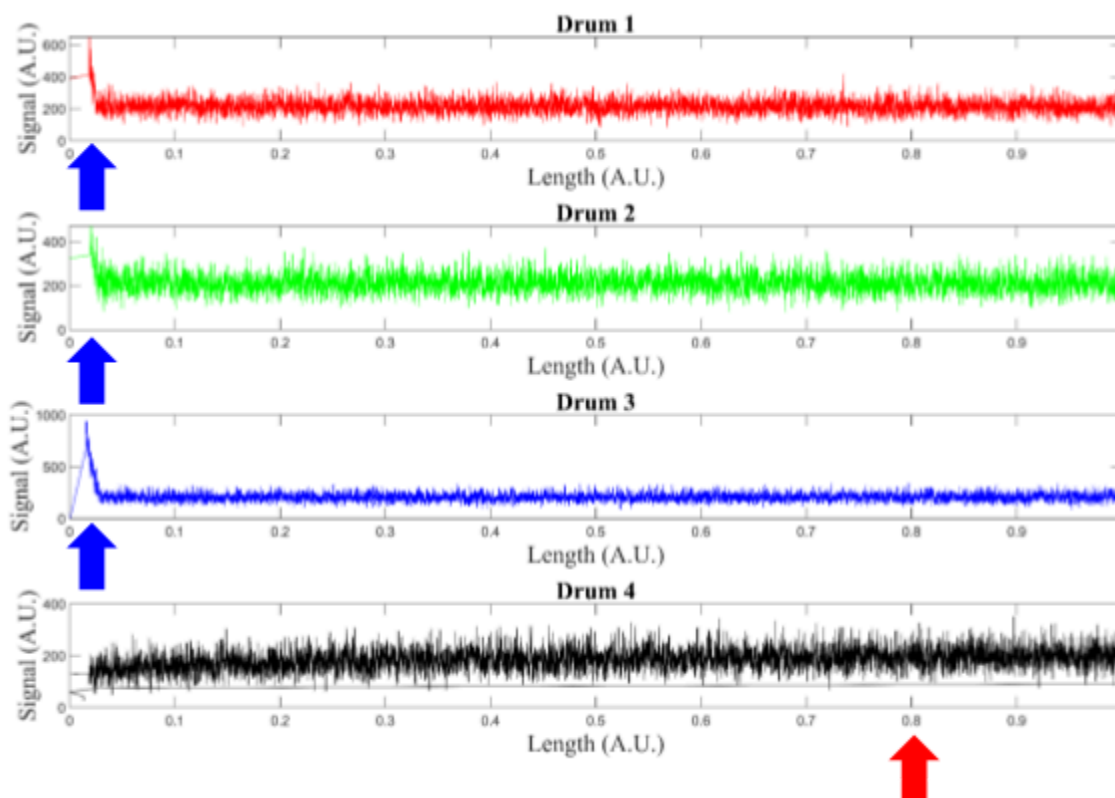

Figure 22. Nickel signal intensity down the length of the mylar collection strip. Nickel particles' mobility size was selected at 200 nm. Blue arrows indicate artifacts of the ICPMS signal spike, and red arrows indicate where the expected peak should be.

Figure 23 shows the lanthanum signals on the mylar strips. This plot is distinctly different from the others, with nearly zero signal for most of the length. There are several points along the line where the signal is greater than zero, but they are sporadic and do not match with where the expected peak should be. This could be a result of quantized noise, which comes about from the translation of the analog signal of ion intensities to a digital signal for processing.
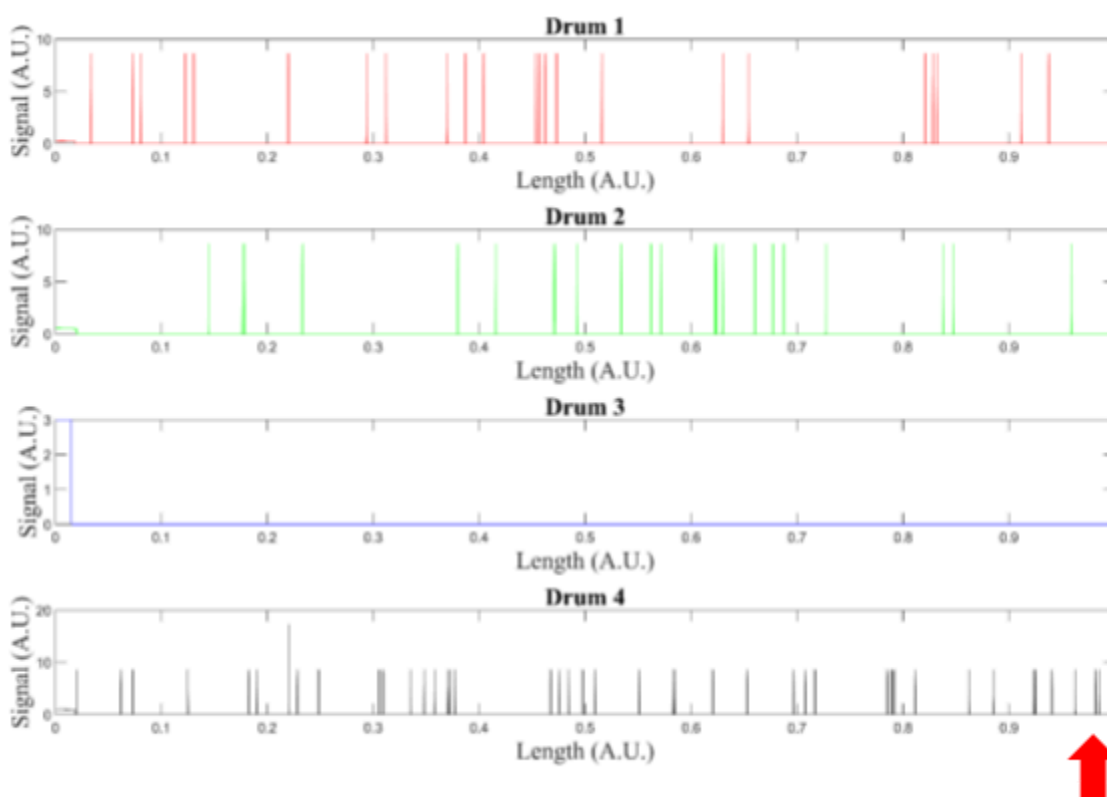

Figure 23. Lanthanum signal intensity down the length of the mylar collection strip. Lanthanum particles' mobility size was selected at 250 nm. Red arrows indicate where the expected peak should be.

In addition to the graphs presented here, a wider range of aerosol sizes were tested using this method (50 nm to 1 μm). All of the sizes did not have a corresponding peak in the ICPMS data, on any of the drums that they were predicted to be on.

Indoor Air Quality Investigation

The following **Figures 24 - 26** are time resolved signals from several tracked elements in the locations where the instrument was deployed. The data was smoothed using the *smooth* MATLAB function, where each point was averaged with the nearest 20 points. There was an unexplained spike in concentration in all LA-ICPMS signals at the very beginning of the strips, which were cut out of data sets as noise, just as with the characterization experiments.

A key feature that it hypothesized to be in these plots is diurnal variation in signal in the PDL and the Kiln room. In the PDL, there are metal working machines, such as CNCs, milling machines, and welding, running during the day, but not at night. It is expected that the Kiln room follows the same pattern. The signal from the outside air should not have much pattern, because it is a relatively clean, well mixed sample of air.

Figure 24 shows the signals from select metal elements in the PDL. There is no diurnal variation in any of the signals, and they appear nearly constant along the length of time collection. There are some signals that are non-zero, but it cannot be determined if

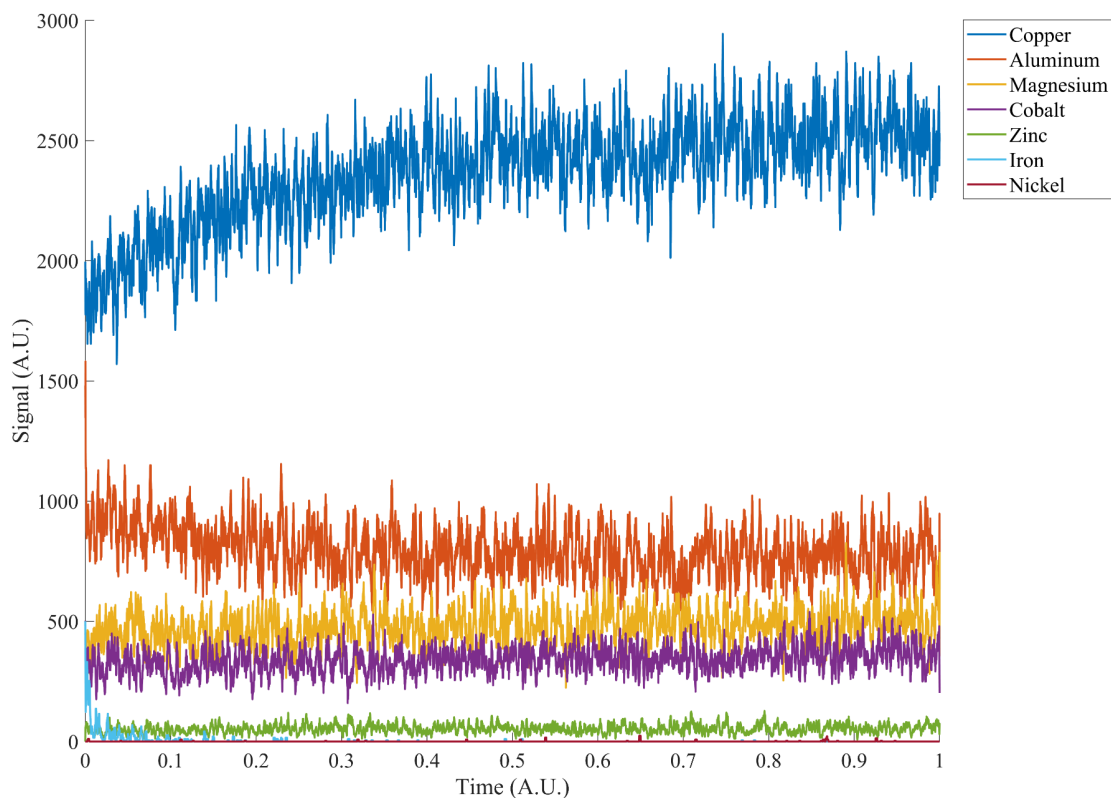they are at unsafe metal levels without transforming the signal to concentration using ICPMS standards.

Figure 24. Combined signals of metal aerosols from all drums over time deployed in the Project Development Lab in Dana Engineering. Deployment time was 1 week.

Figure 25 shows the signals from the same metal elements collected from the run in the Kiln room. Similarly to the PDL data, there are no diurnal signal changes. The

signal strength of the metals is lower than seen in the PDL, which makes sense because there is less metal working equipment in the Kiln room.
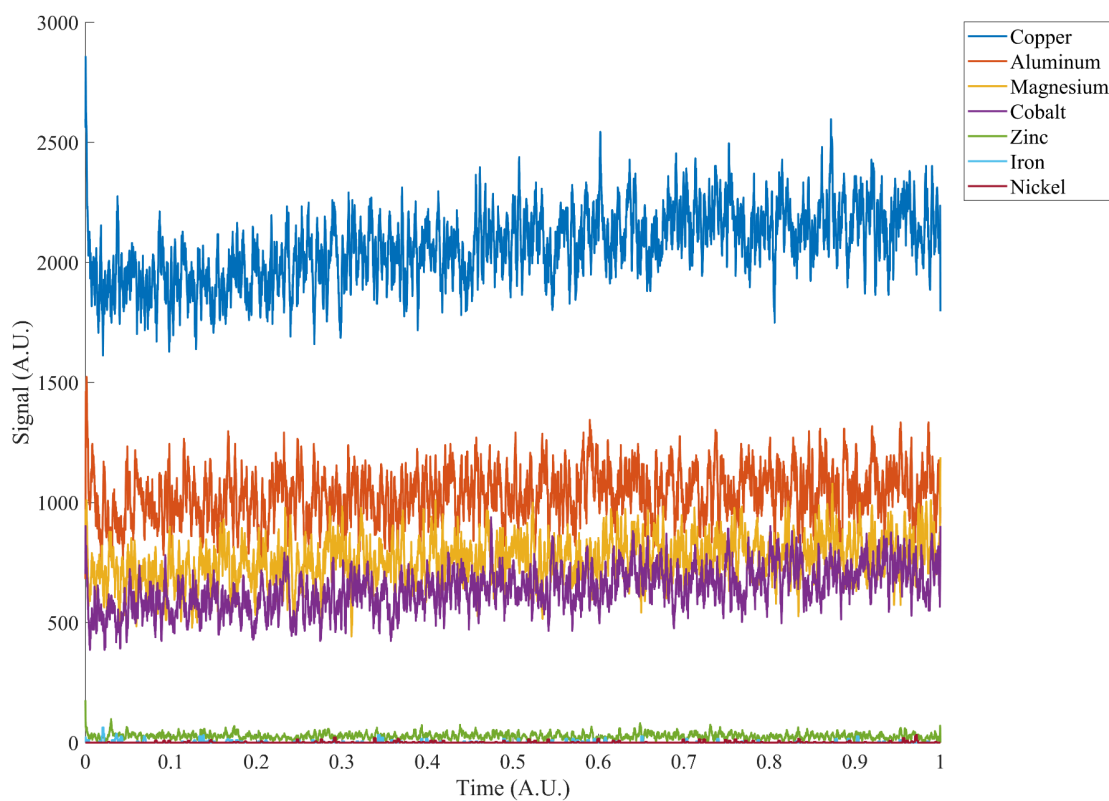

Figure 25. Combined signals of metal aerosols from all drums over time deployed in the Kiln room in 7th Street Makerspace. Deployment time was 1 week.

Figure 26 shows the signals of the metal elements collected outside on the rooftop of Academic East. There is less total signal for all of the metal elements, but there is still non-zero signal of some metals. This does merit some investigation into using ICPMS standards to convert the signal into concentration. A more in depth discussion of future works is given in **Conclusions**.
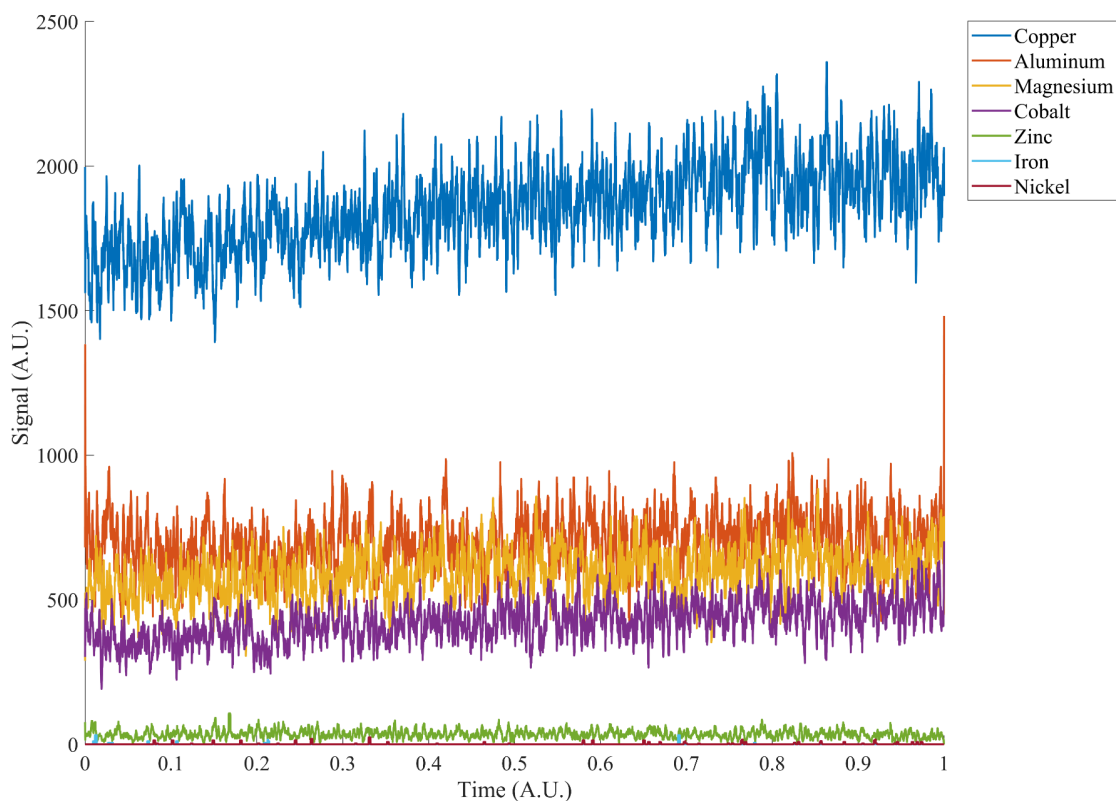

Figure 26. Combined signals of metal aerosols from all drums over time deployed on the rooftop of Academic East. Deployment time was 1 week.

Discussion

Characterization

The **Figures 17 - 23** are all missing peaks that correspond to the location in which the particles impacted. The peak that is expected to be seen is similar to the peak in signal strength at the beginning of the sulfur strip on Drum 4 (**Figure 21**). It is not clear why there was such a strong signal present in this sample, as the predicted cutoff points anticipate that 50 nm particles would not impact.

The lack of signal present on each drum indicates that there is not a significant collection of particles on any of the drums. There are several explanations as to why there is not enough signal detected at the point of impaction to produce a peak. As the DMA separates the particles by electrical mobility, it begins by imparting a charge on the entering aerosols, following the Boltzmann charge distribution. The smaller the particle is, the harder it is to impart a charge on it (**Figure 27**) (Joe et. al., 2018).
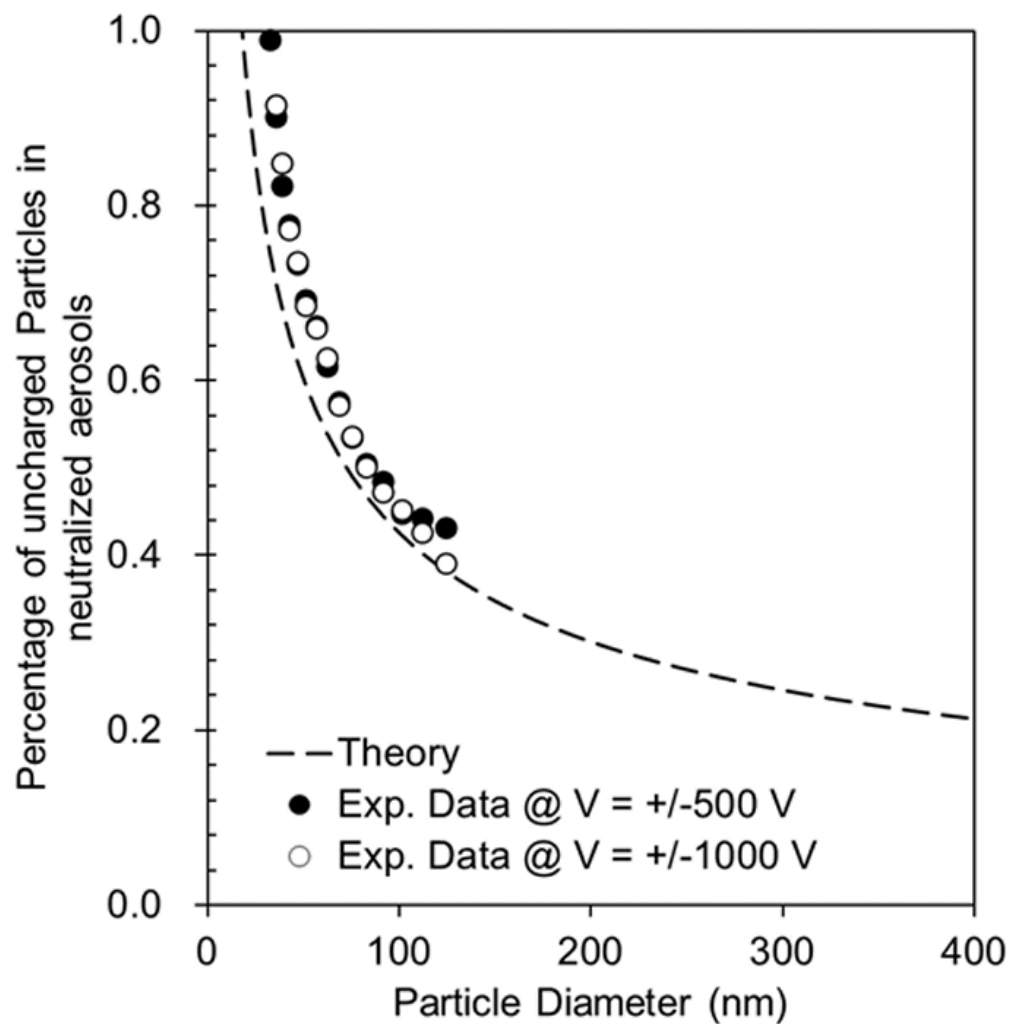
Figure 27. Fraction of uncharged aerosols as a function of particle diameter. The smaller the particle, the less likely it is to be charged by the DMA. Adapted from Y. H. Joe et. al., 2018.

In addition to smaller particles being harder to induce a charge onto, at the point of generation, less smaller particles are generated with uneven charges. It has been shown

that particles generated from liquid solutions have a particle charge that is linear with the size of the generated particles (Forsyth et. al., 1998).

There has been evidence that shows small particles influence the operation of the DMA by widening the transfer function. Along with this, some particles migrate into the window and other size particles migrate out of the window (Mamakos et al., 2007).

A minor contributor to this loss could be Brownian motion. The smaller the particle, the more it experiences Brownian motion, which, depending on the residence time in the DMA can result in losses of particles. When compared to the previously discussed losses, this would be a significantly small proportion of lost particles.

Therefore, the selected size of the particle might be only a fraction of all of the generated particles. These particles must then be successfully charged, which is difficult for smaller (<200 nm) particles, not be diffused or transferred out of the DMA window, and, ultimately, to be impacted on the side of the drums. These combined effects are why there are no observed signal spikes. Another technique that is used for sequential drum samplers is fluorimetry. In this method, fluorescent particles of different sizes are aerosolized and later quantified through a fluorimeter to track particle sizes. This technique should be investigated in future studies to quantify experimental cutoff points.

Additionally, during the operation of the rotating drum sampler, the total pressure drop across the instrument might not have been sufficient to achieve proper critical flow. When this happens, the impaction performance varies greatly from the theoretical performance. A solution to this is to increase the strength of the vacuum pulling flow through the system.

Indoor Air Quality Investigation

The data presented in **Figures 24 - 26** do not show a distinct diurnal pattern of signal strength over the deployment periods. This could indicate that there is no buildup of metal aerosols in the air in any of the following locations. The air outside is well mixed, and as it is deployed from any major sources of pollution, this is an expected result. The lack of diurnal patterns in the PDL and Kiln room, which do not run most equipment overnight, could indicate that the rooms are properly ventilated during equipment use. Future studies should investigate the corresponding signals to time controlled release of metal aerosols.

Further analysis of the copper signal from all three locations show that there is a slight difference in the strengths of the signal in the different locations. If there is no diurnal pattern in signals, and all of the variation present is noise from the LA-ICPMS, there is a difference in the copper signal (**Figure 28**). It is difficult to definitively determine if the difference in signal strength is large enough to be equivalent to a difference in elemental concentration without developing ICPMS standards for the elements and concentrations that are present.
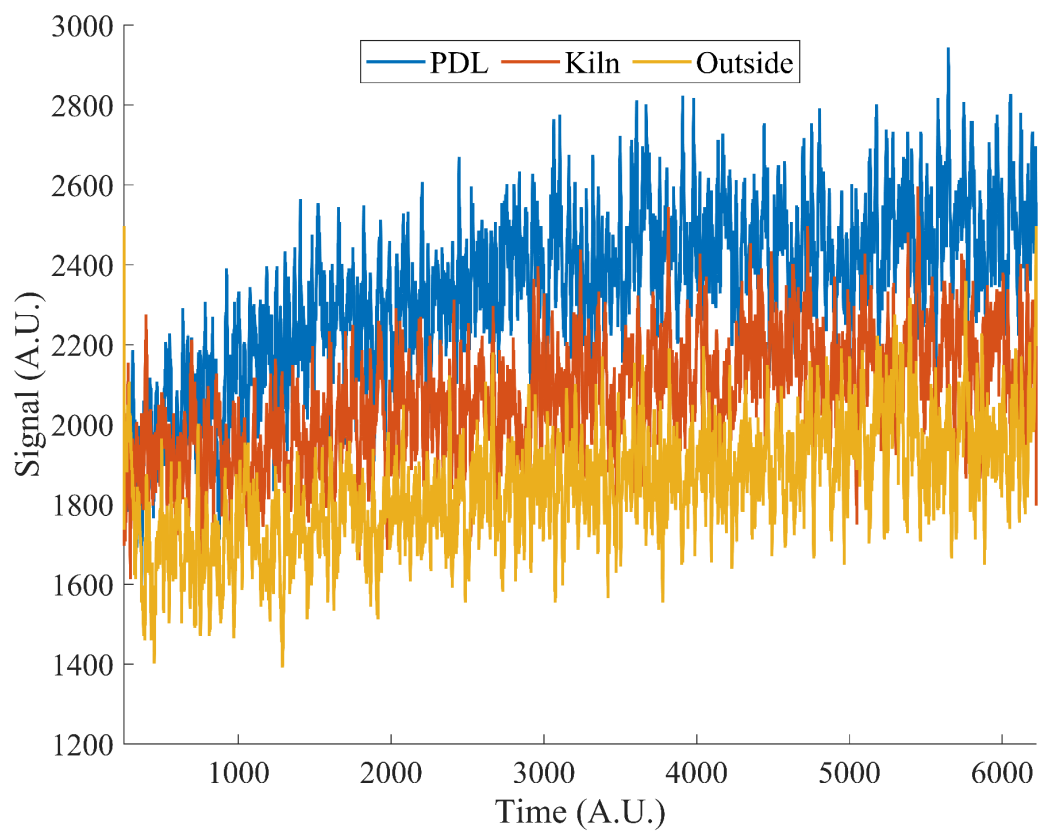
Figure 28. Copper signal over time from all deployment locations.

Conclusion

Although the characterization goal of this thesis did not produce the expected results, the investigation into the cutoff points and persistent communication with the manufacturer elucidated more information about the expected performance of the drum sampler. With the new information provided, the sizes of elemental metal pollution can be tracked during the normal operation of the instrument. From the indoor air quality monitoring goal, there might be a difference in the concentrations of copper concentrations in the PDL and outside air. There does not appear to be a clear diurnal pattern in the makerspaces on campus caused by running equipment during the day according to the way that this data was processed. However, due to the data smoothing that was done, it is plausible that the diurnal patterns are buried in the averaging. Finding the mathematical transformation from time of collection to length on the strip to time collected by the ICPMS is a critical extension to make sure that no signal peaks are missed.

This project is one of the first attempts at monitoring the elemental composition of aerosols with LA-ICPMS using a rotating drum sampler that gives time resolution. Other technologies that can analyze the elemental composition of collected aerosols generally use equipment like a synchrotron beam, which is much more costly than LA-ICPMS. With regards to this, these thesis showed that it is a promising method of air quality monitoring. In order for this work to answer definitive, quantitative questions about the concentration of elemental species at certain times, there are several key

extensions to this work that must be completed. The most important next steps can be done for the characterization of the drum sampler and the LA-ICPMS method of analysis.

With regards to the characterization experiments, to verify that there are enough particles exiting the DMA in the monodisperse stream, the CPC can run on the outlet to count the particles that would be entering the drum sampler. Methods of increasing the amount of particles exiting the DMA should be investigated. Some methods could include working with the larger size range of particles (> 500 nm) for more successful charging, or varying the sheath and aerosol flow rates to widen the transfer function in the DMA. Additionally, to acquire a baseline signal for metal salts on the ICPMS, a solution can be dried on the mylar and analyzed with the LA-ICPMS.

With the amount of trouble that the LA-ICPMS has had over the course of the experiments, it would be beneficial to ensure that the ICPMS is an appropriate method of chemical analysis for the mylar strips. This can be done by allowing the drums to rotate while the atomizer is alternating between aerosolizing a metal salt solution and allowing air to go over. This should be a much clearer "on-off" signal that should be present in the ICPMS signal after analysis.

References

Antunes, Marcelo B., et al. "San Francisco/Oakland Bay Bridge Welder Study."
Neurology, vol. 69, no. 12, Sept. 2007, pp. 1278–84. *neurology.org (Atypon)*,
https://doi.org/10.1212/01.wnl.0000276988.50742.5e.

Cahill, Thomas A., et al. "Analysis of Respirable Fractions in Atmospheric
Particulates via Sequential Filtration." *Journal of the Air Pollution Control
Association*, vol. 27, no. 7, July 1977, pp. 675–78. *Taylor and Francis+NEJM*,
https://doi.org/10.1080/00022470.1977.10470474.

Cahill, Thomas A., et al. "Inorganic and Organic Aerosols Downwind of California's
Roseville Railyard." *Aerosol Science and Technology*, vol. 45, no. 9, Sept. 2011,
pp. 1049–59. *Taylor and Francis+NEJM*,
https://doi.org/10.1080/02786826.2011.580796.

Dockery Douglas W., et al. "An Association between Air Pollution and Mortality in
Six U.S. Cities." *New England Journal of Medicine*, vol. 329, no. 24, 1993, pp.
1753–59. *Taylor and Francis+NEJM*,
https://doi.org/10.1056/NEJM199312093292401.

Fabretti, Jean-François, et al. "ICP-MS Determination of Trace Elements in Aerosols
Using a Dynamic Reaction Cell: First Results in PM10 Comparing Road and
Aerial Traffic in Nice Area (France)." *Annali Di Chimica*, vol. 97, no. 9, Sept.
2007, pp. 875–85. *PubMed*, https://doi.org/10.1002/adic.200790072.

Forsyth, Bruce, et al. "Particle Charge Distribution Measurement for Commonly

    Generated Laboratory Aerosols." *Aerosol Science and Technology*, vol. 28, no.

    6, Jan. 1998, pp. 489–501. *Taylor and Francis+NEJM*,

    https://doi.org/10.1080/02786829808965540.

Hinds, William C. *Aerosol Technology*. 2nd ed., John Wiley & Sons, 1999.

Iannilli, Emilia, et al. "Effects of Manganese Exposure on Olfactory Functions in

    Teenagers: A Pilot Study." *PLoS ONE*, vol. 11, no. 1, Jan. 2016, p. e0144783.

    PubMed Central, https://doi.org/10.1371/journal.pone.0144783.

"Indoor Air Quality." *National Institute of Environmental Health Sciences*,

    https://www.niehs.nih.gov/health/topics/agents/indoor-air. Accessed 28 Mar.

    2024.

Jafek, Bruce W., et al. "Anosmia after Intranasal Zinc Gluconate Use." *American

    Journal of Rhinology*, vol. 18, no. 3, 2004, pp. 137–41.

Joe, Yun-Haeng, et al. "A Study on Electrical Charge Distribution of Aerosol Using

    Gerdien Ion Counter." *Aerosol and Air Quality Research*, vol. 18, no. 12, 2018,

    pp. 2922–28. *aaqr.org*, https://doi.org/10.4209/aaqr.2018.08.0309.

M, Klinger-Strobel, et al. "Aspects of Pulmonary Drug Delivery Strategies for

    Infections in Cystic Fibrosis - Where Do We Stand?" *Expert Opinion on Drug

    Delivery*, vol. Feb 2:., Jan. 2015, pp. 1–24.

Mamakos, Athanasios, et al. "Diffusion Broadening of DMA Transfer Functions.

    Numerical Validation of Stolzenburg Model." *Journal of Aerosol Science*, vol.

38, no. 7, July 2007, pp. 747–63. *ScienceDirect*,

https://doi.org/10.1016/j.jaerosci.2007.05.004.

Marple, Virgil Alan. *Fundamental Study of Inertial Impactors*. COO-1248-21, Univ.

of Minnesota, Minneapolis, MN (United States), 1 Dec. 1970. *www.osti.gov*,

https://doi.org/10.2172/4095434.

Pope, C. Arden. "Epidemiology of Fine Particulate Air Pollution and Human Health:

Biologic Mechanisms and Who's at Risk?" *Environmental Health Perspectives*,

vol. 108, 2000, pp. 713–23. *JSTOR*, https://doi.org/10.2307/3454408.

Raab, O. G., et al. *Deposition of Inhaled Monodisperse Aerosols in Small Rodents*.

Sept. 1975. *escholarship.org*, https://escholarship.org/uc/item/723362jb.

Saleh, Yara, et al. "Exposure to Atmospheric Ultrafine Particles Induces Severe Lung

Inflammatory Response and Tissue Remodeling in Mice." *International Journal*

of Environmental Research and Public Health, vol. 16, no. 7, 7, Jan. 2019, p.

1210. *www.mdpi.com*, https://doi.org/10.3390/ijerph16071210.

TSI. *Series 3080 Electrostatic Classifiers Operation and Service Manual*. Mar. 2009.

https://cires1.colorado.edu/jimenez-group/Manuals/SMPS_3080_manual.pdf

US EPA, OAR. *What Is a HEPA Filter?* 19 Feb. 2019,

https://www.epa.gov/indoor-air-quality-iaq/what-hepa-filter.

What Size Particle Is Important to Transmission of COVID-19? | Aerosol

Laboratory.

https://www.aerosol.mech.ubc.ca/what-size-particle-is-important-to-transmissio

n/. Accessed 28 Mar. 2024.

Zhang, Boya, et al. "Comparison of Particulate Air Pollution From Different

Emission Sources and Incident Dementia in the US." *JAMA Internal Medicine*,

vol. 183, no. 10, Oct. 2023, pp. 1080–89. *Silverchair*,

https://doi.org/10.1001/jamainternmed.2023.3300.

Appendix A

Theoretical Cut-off Point Sample Calculations

Drum 1

$$d_{50}(\mu m) = \left[\frac{9 \cdot 1.824{\cdot}10^{-5}\, Pa{\cdot}s \ \cdot(0.00193\, m)^2{\cdot}0.0095\, m \cdot 0.59}{1000\, \frac{kg}{m^3} \cdot 3.833{\cdot}10^{-4}\, \frac{m^3}{s}} \right]^{0.5} \cdot \frac{10^6 \mu m}{1\, m} - 0.078\, \mu m$$

$$d_{50}(\mu m) = 2.91\, \mu m$$

Drum 2

$$d_{50}(\mu m) = \left[\frac{9 \cdot 1.824{\cdot}10^{-5}\, Pa{\cdot}s \ \cdot(0.00082\, m)^2{\cdot}0.0095\, m \cdot 0.59}{1000\, \frac{kg}{m^3} \cdot 3.833{\cdot}10^{-4}\, \frac{m^3}{s}} \right]^{0.5} \cdot \frac{10^6 \mu m}{1\, m} - 0.078\, \mu m$$

$$d_{50}(\mu m) = 1.19\, \mu m$$

Drum 3

$$d_{50}(\mu m) = \left[\frac{9 \cdot 1.824{\cdot}10^{-5}\, Pa{\cdot}s \ \cdot(0.00030\, m)^2{\cdot}0.0095\, m \cdot 0.59}{1000\, \frac{kg}{m^3} \cdot 3.833{\cdot}10^{-4}\, \frac{m^3}{s}} \right]^{0.5} \cdot \frac{10^6 \mu m}{1\, m} - 0.078\, \mu m$$

$$d_{50}(\mu m) = 0.39\, \mu m$$

Drum 4

$$d_{50}(\mu m) = \left[\frac{9 \cdot 1.824{\cdot}10^{-5}\, Pa{\cdot}s \ \cdot(0.0028\, m)^2{\cdot}0.0095\, m \cdot 0.59}{1000\, \frac{kg}{m^3} \cdot 3.833{\cdot}10^{-4}\, \frac{m^3}{s}} \right]^{0.5} \cdot \frac{10^6 \mu m}{1\, m} - 0.078\, \mu m$$

$$d_{50}(\mu m) = 0.20\, \mu m$$

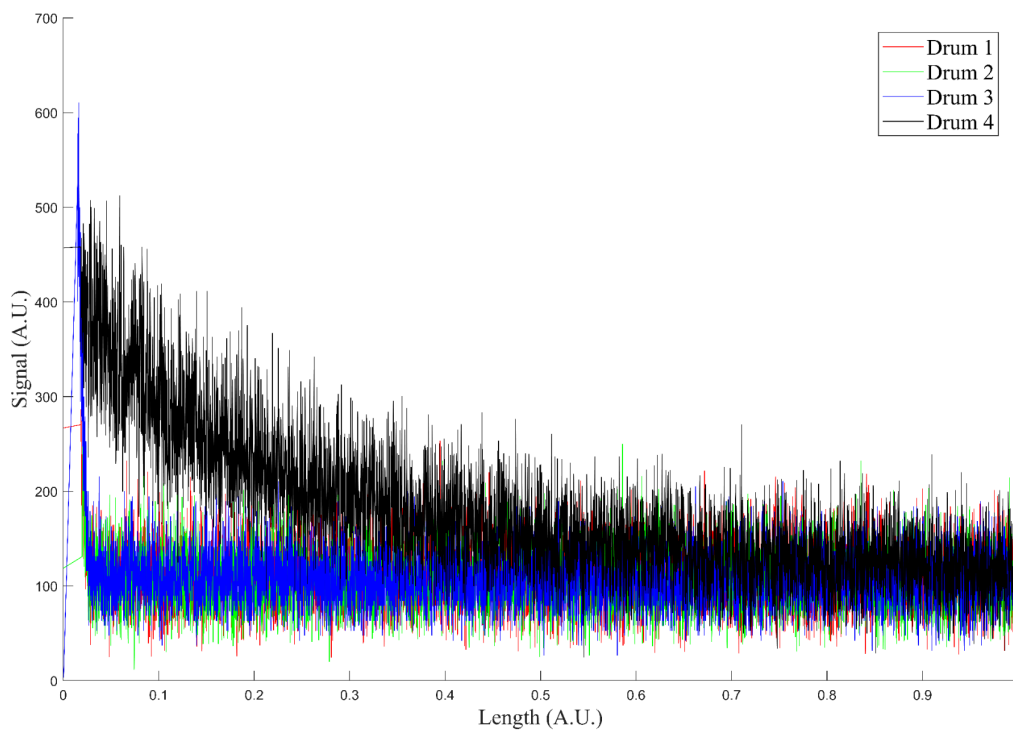*Compiled Drum Data from Characterization Results*

Figure A1. Aluminum signal intensity down the length of the mylar collection strip.

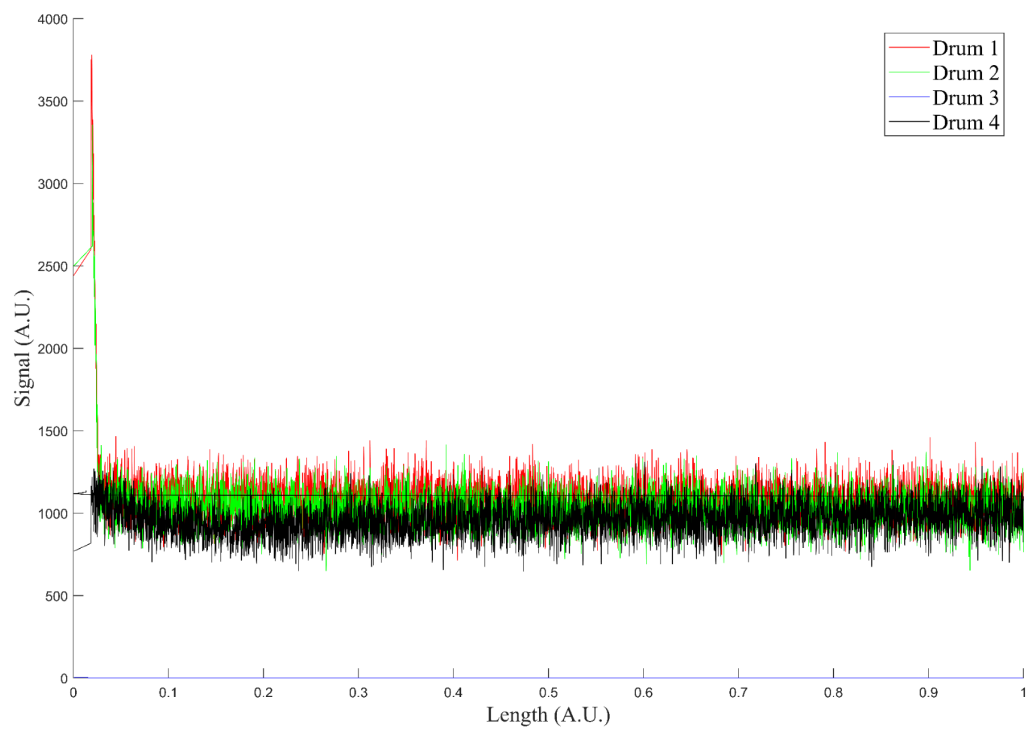Aluminum particles' mobility size was 50 nm.

Figure A2. Chlorine signal intensity down the length of the mylar collection strip.
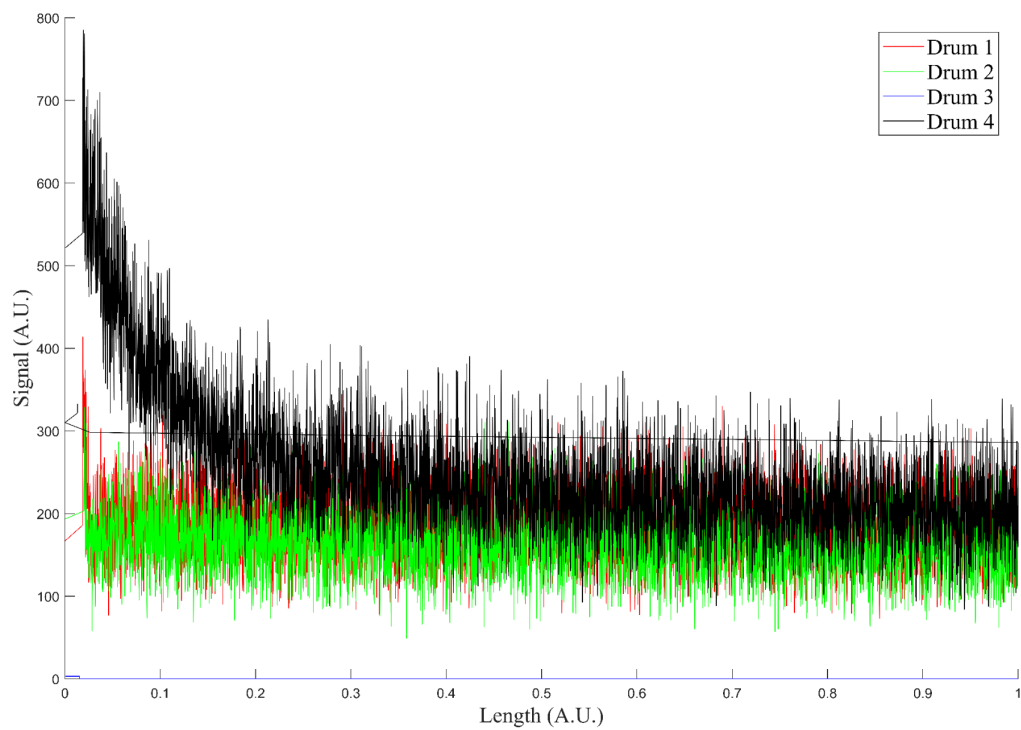
Chlorine particles' mobility size was 100 nm.

Figure A3. Iron signal intensity down the length of the mylar collection strip. Iron particles' mobility size was 100 nm.
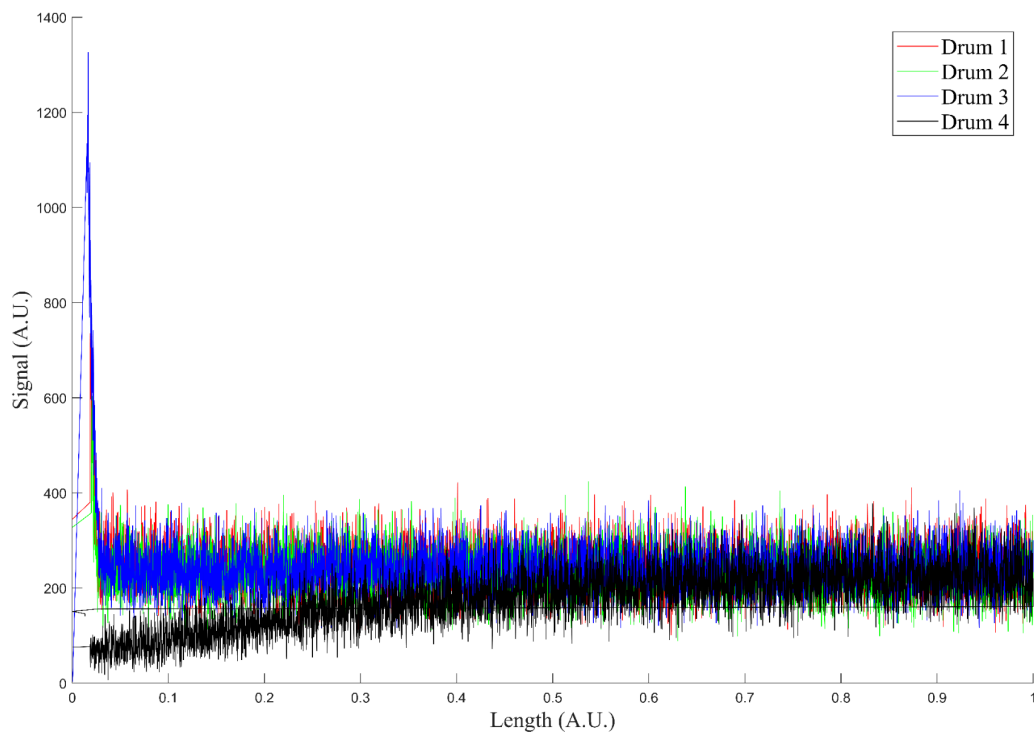
Figure A4. Copper signal intensity down the length of the mylar collection strip. Copper particles' mobility size was 150 nm.
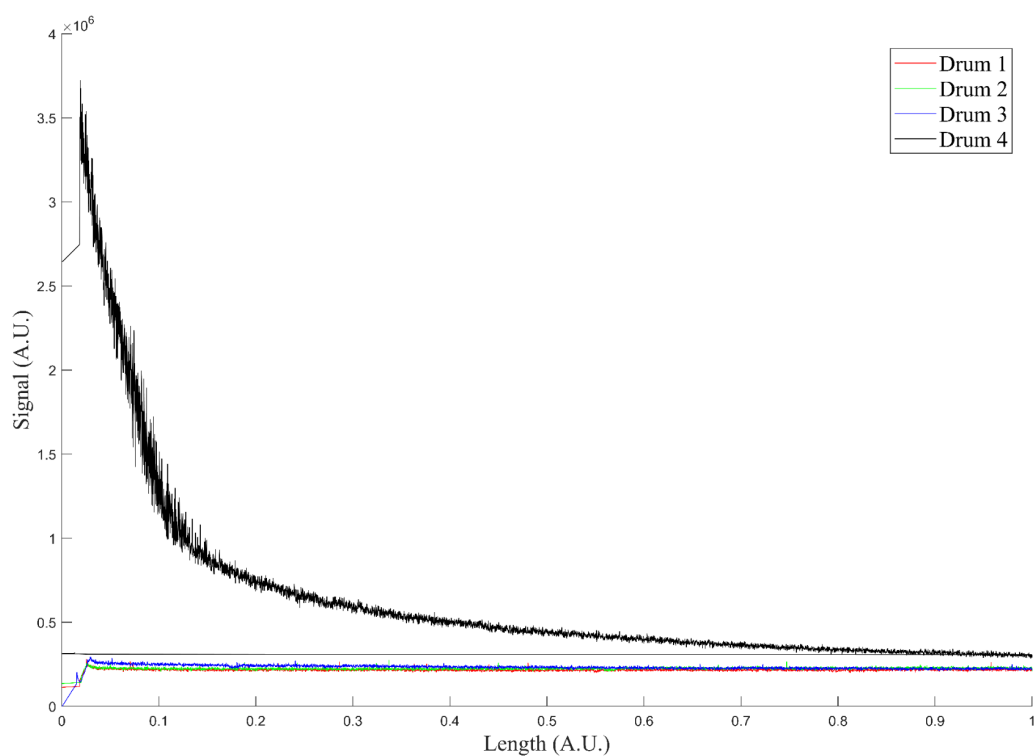
Figure A5. Sulfur signal intensity down the length of the mylar collection strip. Sulfur

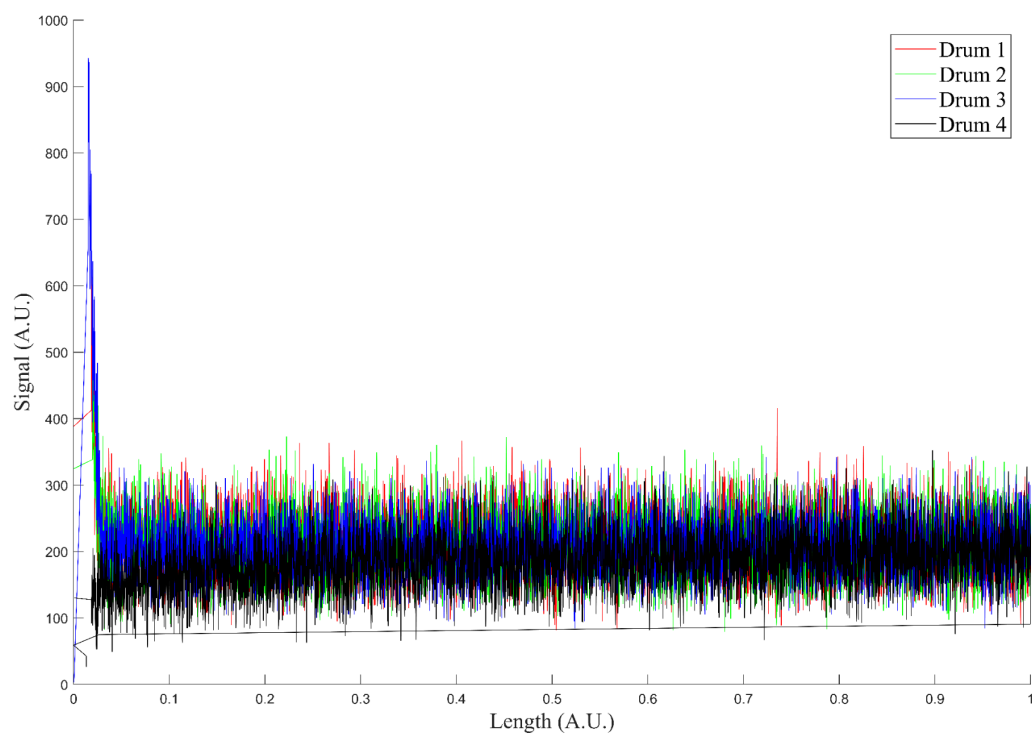particles' mobility size was selected at 50 nm, 150 nm, and 200 nm.

Figure A6. Nickel signal intensity down the length of the mylar collection strip. Nickel particles' mobility size was selected at 200 nm.
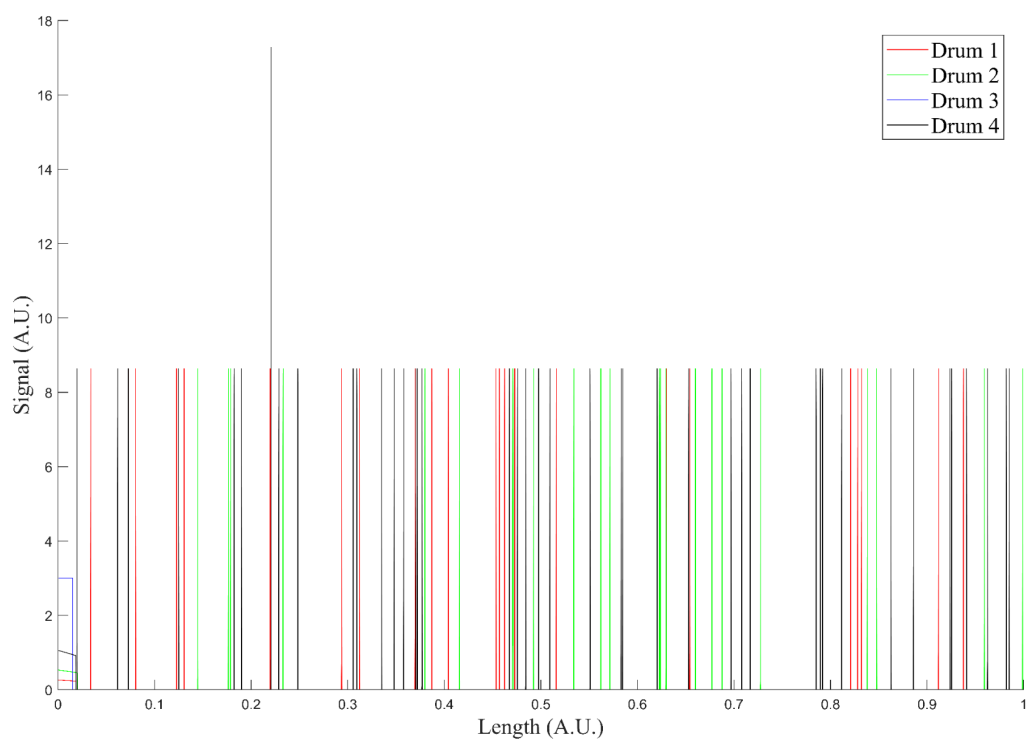
Figure A7. Lanthanum signal intensity down the length of the mylar collection strip.

Lanthanum particles' mobility size was selected at 250 nm.

Appendix B

Appendix B highlights key operating information of the 4 drum sampler used in this thesis.

Drum Air Supplementary Manual

Updated Spring 2024

Written to be read along with the other manual in Netspace; contains what I learned about how to operate it

Power on

- Press the button on the yellow box (on the face towards the pressure gauge) to turn on

- Holding that button for a few seconds will turn it off

- Holding the button after it has already turned off will restart the instrument

Connecting To Instrument

In order to give the instrument commands and collect data, you will need to connect to the drum's Wi-Fi network and visit its IP address

- Wi-Fi network is called 'DRUM8029'

- Password is 'drumsampler'

  - Note: You will not have Internet access while connected to the drum's network

Syncing GPS and Clock

GPS signal needs to be established so that the time and date on the instrument are set. The instrument will begin to connect as soon as it is turned on. The date, time, and GPS status can be checked on the webpage (see next section). The time can

occasionally vary from the true time. Make note of the difference for comparing the data in the drum log.

Commands

To get to the webpage where you can communicate with the instrument, enter '192.168.4.10' into any browser while connected to the drum's Wi-Fi. In the webpage you can enter the command found in the other manual. Note that the commands must be given in UTC, not EST.

● Deploy ID - naming convention is yearmonthday (ex. Feb 14 2022 - 20220214)

● Advance Rel – rotates the drum a defined distance around

● Advance Abs – used to move the drum to a specific location, after SetPosition is used to define one position

● Rotation Rate - max rate from manufacturer website is 24 (mm/day), but can be set higher

● Pump - '1' turns on '0' turns off

● Set Position – can be used to define the current position to a defined value

○ Ex. If the slot is facing the orifice, you can define that position as zero

● Delete Deploy – used to delete all data pertaining to a named Deployment ID

● Shutdown - very slow, ~10 minute delay. I found the button to be better

Download

Downloads a .CSV file through the browser

Internal Components

- 11hs20-0674s-pg100 stepper motor

    - An additional one was ordered and is in the lab

- Yellow Box of Electrical components

    - The yellow box houses all of the batteries and internal circuit boards. The problem that we faced all semester was because the connection between the main computing board and the board that controlled the stepper motor was severed.

    - The pictures below show the insides of the yellow box. On the right side of the box, (**Figure B1**) there are the batteries and packing to keep everything from moving. On the left side, (**Figure B2**) there are two circuit boards and GPS connectors. The board that controls the motor is called "phidget stepper"

Figure B1. Picture of the right side of the electrical components: houses the batteries for the system.
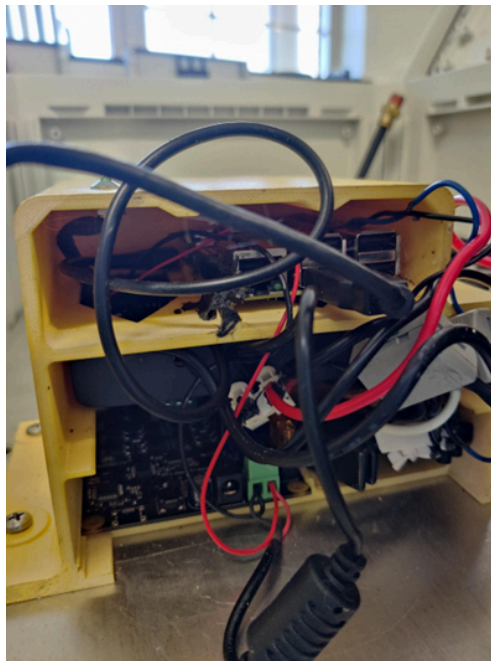

Figure B2. Picture of the left side of the electrical components: houses the control boards